Title: **Statistical significance of notch fatigue prognoses based on the strain-energy–density method: Application to conventionally and additively manufactured materials**

Authors: **M. Benedetti, M. Dallago, C. Santus**

DOI Link: https://doi.org/10.1016/j.tafmec.2020.102720

Statistical significance of notch fatigue prognoses based on the strain-energy-density method: application to conventionally and additively manufactured materials

M. Benedetti[a*], M. Dallago[a], C. Santus[b]

[a]Department of Industrial Engineering – DII, University of Trento, Italy

[b]Department of Civil and Industrial Engineering – DICI, University of Pisa, Italy

*Corresponding author:
Matteo Benedetti
matteo.benedetti@unitn.it

Abstract

The inverse search determination of the strain-energy-density (SED) control radius R_1 devised in *Benedetti et al. Int J Fatigue 2019;126:306-318* and based on the knowledge of the notch fatigue factor estimated using an optimal V-notch specimen geometry is here reformulated to take into account the statistical properties of the input fatigue properties. It was found that R_1 exhibits a non-symmetric probability density function that is well represented by a skew-normal distribution. The uncertainty in R_1 can be attributed to the uncertainty in the inverse search procedure and to the material variability in notch sensitivity. By applying the devised procedure to real experimental data, it was found that the former contribution is preponderant in the assessment of very sharp notches, while the latter dictates the fatigue strength of blunt notches, especially in the case of intrinsically flawed materials, such as those additively manufactured.

Keywords

Strain energy density; notch fatigue assessment; control radius; statistics; additive manufacturing

Nomenclature

AM	Additive manufacturing
CDF	Cumulative distribution function
CV	Coefficient of variation
MC	Monte Carlo
NCV	Normalized coefficient of variation
PDF	Probability density function
SED	Strain energy density
SLM	Selective laser melting
SND	skew-normal distribution
TCD	Theory of critical distances
D	Specimen outer geometry (Fig. 2)

E	Young's modulus
I_1	dimensionless parameter controlling $\Delta\bar{W}_1$ (Eq. (5))
K_f	fatigue stress concentration factor
K_N	notch-stress intensity factor
$K_{N,UU}$	N-SIF for unitary nominal stress and unitary half-diameter D
L	TCD critical distance
m	slope of the linear relationship between R'_0 and R'_1 for perfectly sharp notch
R	notch radius
R	stress ratio
r	CV of plain fatigue strength
r_N	CV of notch fatigue strength
R'_0	dimensionless control radius based on the stress singularity assumption
R'	dimensionless notch radius
r_0	position of the averaging control domain (Fig. 1)
R_1	Mode I SED control radius
R'_1	dimensionless control radius
$\bar{R}'_1$	dimensionless control radius estimated from mean values of plain and notch fatigue strength
$R'_{1,lim}$	control radius corresponding to a given value of NCV ν
R'_{lim}	dimensionless notch radius corresponding to a given value of NCV
s	William's power law singularity exponent
S, S_N	standard deviation of plain and notch fatigue strength, respectively
sk	skewness of dimension-less control radius
α	shape parameter of SND
$\bar{\alpha}$	notch opening half-angle (Fig. 1)
β	location parameter of SND
γ	scale parameter of SND
δ	standard deviation of dimensionless control radius
$\delta(R_1)$	amplitude of the uncertainty interval of R_1
$\Delta\sigma_{fl}$	plain specimen fatigue strength range. In this work, it is assumed to be normally distributed with mean $\Delta\bar{\sigma}_{fl}$ and standard deviation S
$\Delta\sigma_{N,fl}$	plain specimen fatigue strength range. In this work, it is assumed to be normally distributed with mean $\Delta\bar{\sigma}_{N,fl}$ and standard deviation S_N
$\Delta\bar{W}_1$	Mode I SED associated with the fatigue full range

κ	r_N to r ratio
μ	mean of dimensionless control radius
ν	CV of the control radius normalized to the equivalent CV of the input data Σ
ν_0	NCV of the control radius for a perfectly sharp notch
$\bar{\nu}$	Poisson's ratio
Σ	equivalent CV of input data for control radius estimation (Eq. (13))

Best-fit coefficients

$a_1,...,a_4$	skewness inversion function (Eq. (11e))
b_1, b_2	limit control radius (Eq. (15))
c_{ij}	matrix coefficients for control radius inverse search (Eq. (6))
d_{ij}	matrix coefficients for the direct problem (estimation of K_f through Eq. (7))
$f_1,..., f_4$	normalized standard deviation on the estimation of notch fatigue strength (Eq. (22))
m_1, m_2	mean of the control radius (Eq. (18))
$n_1,...,n_4$	NCV of the control radius (Eq. (17))
$s_1,..., s_4$	skewness of the control radius (Eq. (19))

1. Introduction

Notch fatigue prognosis is of considerable importance in the mechanical engineering, as the structural integrity of many machine elements is dictated by the fatigue damage usually initiating from geometrical details, such as shoulders, holes, grooves, weld beads, which act as stress raisers. It is well known that the fatigue response is not so much controlled by the peak stress as by the stress state reigning in a neighborhood of finite size surrounding the critical spot of the component. Different approaches have been proposed so far in the technical literature to account for the material capability of accommodating stress concentrations produced by time-varying loads. The most popular notch fatigue design criteria are based on the definition of a notch sensitivity factor [1] or notch support factor related to the slope of the stress gradient emanating from the stress peak location [2]. More sophisticated fracture mechanics approaches attempt to incorporate also the fatigue life spent to propagate the crack initiated in the critical fatigue location until eventual failure [3,4]. Neuber [5] and Peterson [6] were the first to introduce the key concept of "structural volume": the fatigue crack initiation mechanisms, which takes most of the fatigue life in the high-cycle fatigue regime of mechanical components of medium-to-small size, is controlled by the stress-strain process occurring in a domain of material characteristic size. Their pioneering works paved the way for the theorical framework of notch fatigue assessment approaches based on the concept of averaging in the neighborhood of the notch a fatigue damage parameter representative of the notch stress-strain field. A comprehensive review of these methods is given in

the recent literature review paper [7]. Among them, the Theory of Critical Distance (TCD) was conceptualized by Taylor [8] and Susmel [9] and postulates that the critical condition in a notched or cracked member is achieved when a suitable stress component evaluated at a certain critical distance, or averaged over a domain of a certain critical size, equals a stress value representative of the fatigue failure in a smooth part. An evolution of TCD to explicitly incorporate the stress gradient is the stress field intensity (SFI) approach initially proposed by Yao [10] and then further elaborated in later researches [11,12]. Another method, which is the focus of the present paper, considers the strain energy density (SED) W as the fatigue damage controlling parameter. Sih [13] was one of the first to argue that the structural integrity of cracked and notched member is related to the SED averaged over a critical distance from the point of stress peak. Gillemot [14] calculated the SED required for crack initiation in a unit volume of material. More recently, Lazzarin and Zambardi [15] laid the foundation for SED-based static and fatigue failure criteria. They are based on an accurate definition of the control volume Ω, over which the SED must be averaged and compared with a critical SED value representative of static or fatigue failure [16]. For plane or axisymmetric problems, the control volume simplifies into a circular domain, as schematically illustrated in Fig. 1. Under mode I type of loading, the circular sector encompassing the notch tip is centered in the origin of the curvilinear reference frame used to describe the notch geometry and located at distance r_0 from the notch tip moving along the notch bisector. r_0 is a function of notch radius R and opening angle $2\bar{\alpha}$. Consequently, the circular domain Ω has a radius r_0+R_1, where R_1 is regarded as the "control radius" and is a material dependent parameter.

TCD and SED approaches have been successfully applied to predict the fatigue strength of blunt and sharp notches [12,17], weld joints [18,19], components exposed to fretting fatigue [20,21] or variable amplitude multiaxial loading [22-24], notches embedded in residual stress fields [25,26], notches in elastic-plastic conditions [27,28]. In all these fatigue scenarios, such methods are applied in a deterministic way with the aim of assessing only the average SN curve of the component (50% probability of failure) without accounting for the dispersion in fatigue strength and life. Nevertheless, it is well known that the fatigue damage is intrinsically stochastic in nature due to variations in material properties, defects, geometries and in-service loads. For this purpose, design codes, like Eurocode 3 [29] and FKM [30], provide the designer with a series of partial safety factors to achieve the target reliability. These empirical or semi-probabilistic approaches suffer in general from a high degree of conservatism, often resulting in oversized structures and unnecessary maintenance costs. For this reason, the scientific community is intensively developing probabilistic approaches able to provide a rational way for fatigue design under uncertainty. The research group formed by Fernández-Canteli and collaborators is very active in reformulating, in a stochastic perspective, various fatigue damage parameters to obtain the Weibull percentile curves of diverse structural components [31-33]. Barbosa et al. [34] extended this concept to devise a probabilistic Stüssi fatigue model based on Weibull distribution. The same statistical distribution was considered by Ai et al. [35] to analyze the fatigue life distribution of specimens with different geometries using the highly stressed volume approach. Zhu et al. [36] reformulated the critical plane approach formerly proposed by Fatemi and Socie [37] by incorporating the variability of the material constants of the Coffin-Manson equation. The concept of weakest-link is widely used to account for the statistical variability

in low-cycle fatigue [38], in assessing the mean stress effect [39], in reinterpreting the Kitagawa-Takahashi diagram [40], in estimating the microstructure-sensitivity of the fatigue notch factor [41]. Fracture mechanics approaches encapsulating a stochastic fatigue crack growth rate law have been proposed to estimate the statistical distribution of the fatigue life spent for crack propagation [42,43].

Taking inspiration from this strong interest in providing fatigue assessment methods with a sound probabilistic framework, the present paper is aimed at investigating the sources of uncertainty in the fatigue predictions using the SED approach. In its original formulation, the fatigue criterion states that a notched component is in fatigue critical condition when the average SED of the notched part $\Delta\overline{W}_{1,\text{notch}}$ equals the SED in the plain sample $\Delta\overline{W}_{1,\text{plain}}$ under the same fatigue critical condition:

$$\begin{aligned}
&\Delta\overline{W}_{1,\text{notch}} = \Delta\overline{W}_{1,\text{plain}} \\
&\Delta\overline{W}_{1,\text{notch}} = \frac{1}{\Omega(R_1)}\int_{\Omega(R_1)} \Delta W \, d\Omega \\
&\Delta\overline{W}_{1,\text{plain}} = \frac{1}{2E}\Delta\sigma_{\text{fl}}^2
\end{aligned} \tag{1}$$

Where E is the Young's modulus, $\Delta\sigma_{\text{fl}}$ the full range plain fatigue limit and Ω is a function of the control radius R_1. From a first inspection of Eq. (1), it is clear that most of the variability in the SED predictions is associated to the scatter in the plain fatigue limit used to estimate the right-hand side part of the equality. In reality, there is also a second and non-negligible source of variability related to the uncertainty in the size of the control radius R_1. This material property is in general indirectly deduced from the fatigue characteristic of a cracked or notched specimen geometry through inversion of Eq. (1). The drawbacks of inferring the control radius R_1 and the critical distance L from the crack growth threshold ΔK_{th} have been already discussed in [44,45]: (i) though precisely described in the ASTM standard [46], the determination of ΔK_{th} is experimentally challenging, especially with negative load ratios, and very susceptible to the precracking procedure and environmental conditions [47,48]; (ii) the fatigue crack growth test is usually performed on a very few samples, more frequently on a single specimen, thus without a sound statistical significance; (iii) this approach cannot be extended to the medium cycle fatigue regime as it is not clear which fracture mechanics parameter is representative of the crack growth resistance in the finite life regime. For these reasons, we devised an inverse search procedure starting from a notched specimen geometry to get a robust assessment of L [44] and R_1 [45]. Specifically, the notch depth of an axisymmetric V-notched specimen was designed to maximize the intensity of the notch singular stress term in order to minimize the sensitivity of the inverse search to experimental uncertainties. Recent investigations [49] about the statistical distribution of the inverse estimation of L pointed out the crucial role played by the notch radius R: the coefficient of variation (CV, standard deviation to mean ratio) of L depends, as expected, on the CV of the input quantities, viz. the plain and notch fatigue strength, and is amplified by a factor that is an increasing function of the ratio R/L. As already observed in [49,50], it is clear that reliable fatigue assessments are only possible when the notch geometry used to get L or R_1 is considerably sharper than that of the notch to be calculated.

The present paper is aimed at extending the investigations done in [49] on the critical distance L to the statistical distribution of the inverse estimation of R_1. The key concept that we want to develop here is that the amplitude $\delta\left(R_1\right)$ of the uncertainty interval of R_1 (also graphically shown in Fig. 1) can be thought of as being composed of two contributions:

$$\delta\left(R_1\right) = \delta\left(R_1\right)_{\text{inversion}} + \delta\left(R_1\right)_{\substack{\text{material}\\ \text{variability}}} \tag{2}$$

Where the first term is related to the uncertainty directly involved in the inversion procedure, for instance due to geometrical inaccuracies (especially on the notch radius) and deviations of the experimental conditions from the nominal ones (sample misalignment, accuracy in load control, etc.). The second term $\delta\left(R_1\right)_{\substack{\text{material}\\ \text{variability}}}$ is the sought material-related variability of R_1. This can be interpreted as the variability in the notch sensitivity of the material (directly correlated to R_1) associated to fluctuations in microstructural features, mechanical properties and defectiveness. Regarding this last issue, it is commonly accepted that intrinsecally defected materials, like cast irons [51] and additively manufactured materials [52], display a lower notch sensitivity. As shown in [41], fluctuations in the size of the critical defect in the vicinity of a notch are associated to a variability in the notch fatigue factor. It is reasonable to expect, and this will be matter of investigation in the present paper, that the first uncertainty term is predominant in the fatigue assessment of very sharp notches, while the second term becomes more evident in the prediction of blunt notches, especially if embedded in materials with significant fluctuations in the fatigue properties.

The present article is organized as follows. Section 2 summarizes the inverse search procedure devised in [45] to deduce the control radius R_1 from plain and notch fatigue strength. Section 3 investigates the statistical properties of R_1 starting from the stochastic characteristics of the input quantities. The impact of the variability of R_1 on the notch fatigue predictions is evaluated in Section 4. Section 5 shows the application of these concepts to the probabilistic fatigue assessment of a conventionally manufactured aeronautical Al-grade and an additively manufactured Ti-alloy. Concluding remarks and directions for future research are given in Section 6. The appendix describes the use of editable Matlab scripts attached to the online version of this paper for a fast implementation of the inverse search and the statistical analyses.

2. Background: inverse determination of the control radius

The procedure recently devised in [45] for an accurate estimation of the control radius R_1 is based on the knowledge of the fatigue strength $\Delta\sigma_{\text{fl}}$ and $\Delta\sigma_{\text{N,fl}}$ of two specimen geometries: the former is regarded as plain and introduces a negligible stress concentration effect, the latter is an axisymmetric V-notched bar, whose geometry is shown in Fig. 2a: A is the notch depth, R is the notch radius, $2\bar{\alpha}$ is the notch opening angle and D is the outer diameter of the specimen. The non-dimensional notch depth $A/(D/2) = 0.3$ was designated in [44] to maximize the intensity of the notch tip singular stress term and hence to minimize the sensitivity of the inverse search of R_1 to the experimental uncertainties. In this way, the only independent specimen dimensions

are D, R and $2\bar{\alpha}$. To keep the problem non-dimensional, the notch root radius and the control radius are normalized with respect to the specimen outer radius:

$$R' = \frac{R}{D/2}; \quad R_1' = \frac{R_1}{D/2} \tag{3}$$

Fig. 2b illustrates the infinitely sharp notch specimen configuration used to get a first estimation of the control radius, here denoted as R_0'. The singular stress distribution is expressed by:

$$\sigma_y(x) = \frac{K_N}{x^s} \tag{4}$$

where K_N is the (net) notch stress intensity factor (N-SIF), and s is the Williams power law singularity exponent. In this way, R_0' can be expressed as:

$$R_0' = \left(\frac{K_{N,UU}}{K_f} \sqrt{\frac{\pi I_1}{(1-s)(\pi-\bar{\alpha})}} \right)^{1/s}; \quad K_f = \frac{\Delta\sigma_{fl}}{\Delta\sigma_{N,fl}} \tag{5}$$

$K_{N,UU}$ is the dimensionless (normalized) N-SIF, for unitary nominal stress and unitary scaling length, i.e. when the specimen outer radius $D/2$ equals unity. $K_{N,UU}$ and s are reported in Table 1 as a function of two notable values of the notch opening angle $2\bar{\alpha}$, viz. 90° and 60°, along with the dimensionless parameter I_1. The fatigue stress concentration factor K_f, obtained as the ratio between the fatigue strength of the two specimen geometries, is the only experimental input of the procedure, besides the notched specimen geometry dimensions.

Figure 2c reports the main formulas to evaluate the dimensionless control radius R_1' from the asymptotic approximation R_0':

$$R_1'(\bar{\alpha},\bar{\nu},R') = m(\bar{\alpha},\bar{\nu})R_0' + \sum_{i=1}^{4}\sum_{j=1}^{5} c_{ij}(\bar{\alpha},\bar{\nu}) R'^{\frac{j}{2}} R_0'^{1-\frac{i}{2}} \tag{6}$$

Where $m(\bar{\alpha},\bar{\nu})$ is the angular coefficient of the linear relationship found in [45] between R_0' and the actual control radius R_1' for the perfectly sharp V-notched specimen. It depends on the notch angle $2\bar{\alpha}$ and the Poisson's ratio $\bar{\nu}$ and its best-fit estimations are listed in Table 1. The coefficients c_{ij} take into account the effect of the notch radius R' in the case of radiused V-notched specimens. They can be obtained by best-fitting the results of FE simulations carried out in [45]. In this previous work, in order to keep the fitting accurate also in the region of low R_1' values, the error variance to be minimized was normalized with respect to each data point. In the present paper, this fitting procedure was repeated by normalizing the error variance with respect to the square of the input data. Specifically, the Levenberg Marquardt algorithm [53] was used to solve the nonlinear fitting problem. The results of this new fitting are provided in the text file and implemented in the Matlab script attached to the online version of this paper. Its use is explained in detail in the Appendix.

The advantage of this new fitting is evident by looking at the relative error maps reported in Fig. 3a and b for $2\bar{\alpha}$=90 and 60°, respectively: the absolute relative error is below 1.5% and more homogeneuosly distributed over the fitting domain as compared to the fit performed in [45].

In the so-called *direct problem*, the input and output variables of Eq. (6) are reversed. In this way, it is possible to deduce R'_0 from the knowledge of R'_1 according to the following equation:

$$R'_0\left(\bar{\alpha},\bar{\nu},R'\right)=\frac{R'_1}{m\left(\bar{\alpha},\bar{\nu}\right)}+\sum_{j=1}^{5}d_{1j}\left(\bar{\alpha},\bar{\nu}\right)R'^{\frac{j}{2}}+\sum_{i=2}^{4}\sum_{j=1}^{5}d_{ij}\left(\bar{\alpha},\bar{\nu}\right)R'^{\frac{j}{2}}R_1'^{\frac{i}{2}} \tag{7}$$

whence, through the inversion of Eq. (5), it is possible to determine the notch fatigue factor K_f:

$$K_f=\frac{K_{N,UU}}{R_0'^{s}}\sqrt{\frac{\pi I_1}{\left(1-s\right)\left(\pi-\bar{\alpha}\right)}} \tag{8}$$

The new fitting coefficients d_{ij} of Eq. (7) are provided in the text file and implemented in the Matlab script attached to the online version of this paper.

3. Statistical properties of the control radius

3.1 The skew-normal distribution

On the base of the comments made in the Introduction, it can be noted that R'_1 is expected to be a function of two random variables, viz. plain $\Delta\sigma_{fl}$ and notch fatigue strength $\Delta\sigma_{N,fl}$. More specifically, R'_1 depends, through complex nonlinear relationships expressed by Eqs. (5,6), on the notch fatigue factor K_f, thus on the ratio of two random variables. We came to a similar conclusion when analysing in [49] the statistical properties of the inverse search estimation of the critical distance L. In this paper, we will follow a similar approach to get the statistical properties of the SED control radius R'_1. The complex formulation of Eqs. (5,6) makes an analytical derivation of the statistical distribution of R'_1 unfeasible, unless a simplified approach is taken. The first simplification concerns the hypothesis that $\Delta\sigma_{fl}$ and $\Delta\sigma_{N,fl}$ are Gaussian (*normal*) random variables. A careful reader might object that the distribution of fatigue strength data is restricted to positive real values, and therefore displays rather a log-normal or, according to the weakest-link concept [35], a Weibull distribution. Nevertheless, we deem the assumption of normally distributed fatigue strength still reasonable for the following reasons: (i) as shown in the following, the analysis is restricted to low CV values (less than 0.1), thus making the occurrence of negative values extremely unlikely and the normal distribution very similar to the log-normal one, (ii) the very commonly adopted (especially in the industrial field) stair-case procedure assumes the fatigue limit to be normally distributed [54]; (iii) the present analysis can benefit from the findings of the research community concerning the distribution of the ratio between two normal variables. We are not aware of similar investigations on differently distributed variables. Ref. [55] investigated the distribution of the ratio between two Weibull random variables, but the analysis is restricted to integer values of the shape parameter of the distribution.

The second simplification involves the use of the Monte Carlo (MC) method to infer the statistical properties of R_1'. This is based on the generation of a (large) population of individuals through repeated random sampling ("trials"). In each trial, individuals of R_1' are randomly generated assuming a Gaussian probability distribution function (PDF) for $\Delta\sigma_{fl}$ and $\Delta\sigma_{N,fl}$. Their mean value and standard deviation are denoted as $\Delta\bar{\sigma}_{fl}$, S, $\Delta\bar{\sigma}_{N,fl}$, S_N, respectively. The corresponding CV are defined as follows:

$$r = \frac{S}{\Delta\bar{\sigma}_{fl}}; \quad r_N = \frac{S_N}{\Delta\bar{\sigma}_{N,fl}} \tag{9}$$

In the MC simulations, the mean value $\Delta\bar{\sigma}_{N,fl}$ is expressed as a function of the input value $\bar{R}_1'$ of the critical radius.

$$\Delta\bar{\sigma}_{N,fl} = \frac{\Delta\bar{\sigma}_{fl}}{K_f\left(\bar{R}_1'\right)} \tag{10}$$

where the fatigue notch concentration factor K_f is calculated according to Eq. (8). $\bar{R}_1'$ represents the control radius estimated considering the average values $\Delta\bar{\sigma}_{fl}$ and $\Delta\bar{\sigma}_{N,fl}$.

In the following, the statistical properties of R_1' will be inferred from populations composed of 100,000 individuals, a number found in [49] to be adequate to get stationary statistical characteristics. The simulations were done considering values of Poisson's ratio $\bar{\nu}$ ranging from 0.27 to 0.33. No detectable influence of $\bar{\nu}$ was found on the statistical properties of R_1', therefore this material parameter will be disregarded in the ensuing discussion.

Figure 4a shows the PDF histograms obtained by elaborating the R_1' populations generated at different values r of the CV of the plain fatigue strength ranging from 0.01 to 0.1. For the moment, we will assume that the notch fatigue strength takes the same CV $r_N = r$, this assumption will be then removed in the following. Interestingly, the PDF is unimodal with longer right-sided tail. The asymmetry degree of the PDF, which can be quantified in terms of skewness (positive in the case of longer right tails), increases with rising r. Figure 4b compares the PDF histograms generated for the nondimensional critical length l (normalized with respect to the specimen outer radius) producing the same fatigue notch factor in the notched sample of same geometry as that considered in Fig. 4b. The PDF of l and R_1' are very similar, with the important difference that the positive skewness of l increases more rapidly with r as compared to R_1'.

As already observed in [49], as long as r is sufficiently small, the PDF histograms of l are well represented (solid lines) by a tri-parametric skew-normal distribution (SND) able to take into account the asymmetry in the PDF visible in Fig. 4 and expressed as [56]:

$$PDF(x) = \frac{1}{\sqrt{2\pi}\,\gamma}\left(1+\operatorname{erf}\left(\frac{\alpha(x-\beta)}{\sqrt{2}\,\gamma}\right)\right)\exp\left(-\frac{(x-\beta)^2}{2\gamma^2}\right) \tag{11a}$$

The same property holds true also for the PDF histograms of R_1' plotted in Fig. 4a (solid lines). Mean μ, standard deviation δ and skewness *sk* of SND are expressed, in contrast to other PDFs (for instance log-normal and Weibull), by simple algebraic functions of shape α, location β and scale γ parameters:

$$\mu = \beta + \frac{\sqrt{\frac{2}{\pi}}\,\alpha\,\gamma}{\sqrt{1+\alpha^2}} \tag{11b}$$

$$\delta = \gamma\sqrt{1-\frac{2\alpha^2}{\pi(1+\alpha^2)}} \tag{11c}$$

$$sk = \frac{\sqrt{2}(4-\pi)\,\alpha^3}{\left(\pi+(\pi-2)\,\alpha^2\right)^{3/2}} \tag{11d}$$

The skewness *sk* is a function of the only shape parameter α and zeroes for vanishing α. In this case, the SND becomes normal with mean β and standard deviation γ. As shown in Fig. 5a, *sk* increases monotonically with α and is bounded in the interval (-1,1). This means that the SND is able to reproduce only PDF with low-to-moderate *sk* values. This explains the reason why the SND fails to correctly represent the PDF of *l* (Fig. 4b) for large values of *r* (above 0.07): when *sk* approaches the unity, α increases asymptotically leading to the degeneration of the PDF evident in Fig. 4b for *r*=0.1. Interestingly, the slower increment of *sk* displayed by R_1' with rising *r* makes the SND suitable to correctly represent the PDF of R_1' even at higher values of *r* (see the plot at *r* =0.1 shown in Fig. 4a). This has the great advantage that the present statistical approach is applicable to materials displaying more dispersed fatigue properties, as discussed in the following, which cannot be analized using the TCD statistical approach proposed in [49]. The following statistical analysis of R_1' will be anyway restricted to *r* values not exceeding 0.1 in order to keep reasonable the hypothesis of normally distributed input fatigue properties discussed at the beginning of this section.

The algebraic inversion of Eq. (11d) to get the shape parameter α from *sk* is computationally very challenging. Therefore, we proposed in [49] the following approximate numerical expression restricted in the positive interval of *sk*:

$$\alpha = \frac{1}{\sqrt{1-sk^2}}\sum_{i=1}^{4} a_i\, sk^{i/2};\ 0 \le sk \le 1 \tag{11e}$$

whose best-fit coefficients a_i are listed in Table 2. As shown in Fig. 5b, the agreement between numerical and analytical solution is very good. Once α has been calculated from Eq. (11e), β and γ can be simply evaluated from Eqs. (11b)-(c).

The hypothesis of normally distributed input fatigue properties with low CV value permits now to extend the above analysis to scenarios in which plain and notch fatigue strength display different CV values *r* and r_N, respectively. For this purpose, we first introduce the following index:

$$\kappa = \frac{r_N}{r} \tag{12}$$

Which quantifies the deviation from the previous assumption of equal CV (κ=1). Recent investigations [57] about the distribution of the ratio Z=X/Y of normal variables with CV r_x and r_y is nearly Gaussian (in reality we already know that its skewness is non-zero) with CV equal to $\sqrt{r_x^2 + r_y^2}$. If this property can be extended to the PDF of R_1' as well, we expect that the PDF in the case of different values of r and r_N is identical to that obtained under assumption of κ=1 provided that both input fatigue properties have the following equivalent CV:

$$\Sigma = \sqrt{\frac{r^2 + r_N^2}{2}} = r\sqrt{\frac{1+\kappa^2}{2}} \tag{13}$$

In fact, the CV of the ratio of two normal variables of same CV Σ will be $\sqrt{r^2 + r_N^2}$ as that of the original problem. To check the validity of the proposed method to deal with scenarios with non-unitary κ values, Figure 4c and 4d compare the actual and equivalent (approximated) PDF of R_1' in the lower and upper bound of the proposed validity range of the index κ: $0.5 \le \kappa \le 2$. Importanty, the agreement in CV between the two distributions is good, being the relative absolute difference below 3%. Additional analyses will be done in the following to confirm the satisfactory accord between actual and equivalent PDF. In this way, it is possible to greatly simplify the statistical analysis of R_1', as its CV can be directly deduced with good accuracy from the only knowledge of Σ. A closer inspection of Fig. 5c and d reveals that the two distributions differ in mean and, to an even greater extent, in skewness (particularly pronounced in the case of low values of κ). Correction functions will be derived in the following to fix this discrepancy.

3.2 Parameters of the skew-normal distribution of R_1'

Parametric MC simulations were carried out to investigate the dependency of mean μ, CV δ/μ and skewness *sk* of R_1' upon the statistical properties of the input fatigue data Σ and κ as well as the geometrical parameters of the notched specimen $2\bar{\alpha}$ and R'. The following discussion will be focused on the notch angle $2\bar{\alpha} = 90°$. Similar considerations hold true also for $2\bar{\alpha} = 60°$. Therefore, no mention will be made in the following about this second notch angle value, apart from reporting in the next tables the corresponding best-fit coefficients.

We will indicate the CV of R_1' normalized to the equivalent CV Σ of the input fatigue data as the normalized coefficient of variation (NCV) expressed by:

$$\nu = \frac{1}{\Sigma}\frac{\delta}{\mu}; \quad \nu_0(\bar{\alpha}) \le \nu \le 7 \Rightarrow \bar{R}_1' = R_{1,\lim}' \tag{14}$$

Figure 6a shows the results of parametric MC runs exploring the effect of notch radius R' and control radius R_1' on NCV ν. Importantly, the NCV is fairly independent of Σ, thus indicating that the CV δ/μ scales linearly with Σ. NCV is greatly influenced by the ratio R_1'/R', in fact it declines with increasing values of R_1' and decreasing values of R'. The lower bound of NCV is set by the condition of infinitely sharp notch ($R' = 0$,

black dashed line in Fig. 6a), which permits to minimize the CV of the estimation of R_1' as it represents the condition of steepest stress gradient. This minimum value of NCV will be indicated as ν_0 and reported in Table 3 for the two explored $2\bar{\alpha}$ values. It is clear that the use of radiused notch geometries will result in R_1' affected by larger values of ν. The higher the notch radius R' in comparison with R_1', the larger the corresponding value of ν.

An effective way of eliminating the dependency upon R' is to research the *locus* of notch radii leading to a fixed value of ν [49]. The grey dashed lines of Fig. 6a indicate the discrete integer values, comprised between 4 and 7, here explored besides the lower bound ν_0. Results at higher ν values are not shown as they lead to excessively dispersed R_1' estimations. Dotted values of Fig. 6b indicate the numerically computed roots of Eq. (14), graphically representing the intersection points of solid curves of Fig. 6a with the horizontal dashed lines ν = *const*. These roots turned out to be independent of Σ and represent the sought *locus* of notch radii R' corresponding to a fixed ν value of NCV. It is well expressed by the following quadratic polynomial (solid lines in Fig. 6b):

$$R'_{1,\lim} = b_1\left(\bar{\alpha},\nu\right)R' + b_2\left(\bar{\alpha},\nu\right)R'^2 \tag{15}$$

Whose best-fit coefficients are listed in Table 4. Importantly, $\bar{R}_1'$ input values satisfying the equality $\bar{R}_1' = R'_{1,\lim}$ are affected by a NCV value ν with a degree of approximation that can be inferred by inspection of Fig. 6c: the NCV evaluated from MC simulations done by keeping fixed ν (=5 in Fig. 6c) and adjusting the value of $\bar{R}_1'$ according to the explored notch radius (Eq. (15)) fall within a relative error band across ν comprised between -1.5% and 3%, irrespectively of the statistical properties Σ and κ of the input fatigue data. This result is very important, as it confirms the ability of Eqs. (13,14) to bring the NCV of R_1' for a generic set of input fatigue data back to that predicted for κ=1 (r=r_N).

Eq. (15) can be easily inverted to get the notch radius $R'_{\lim}$ the NCV of R_1' equal to a prescribed ν value:

$$R'_{\lim} = \frac{-b_1\left(\bar{\alpha},\nu\right) + \sqrt{b_1\left(\bar{\alpha},\nu\right)^2 + 4b_2\left(\bar{\alpha},\nu\right)\bar{R}_1'}}{2b_2\left(\bar{\alpha},\nu\right)}; \quad R_{\lim} = \frac{D}{2}R'_{\lim} \tag{16}$$

The statistical properties of R_1' will be now investigated for five discrete values of ν, namely ν_0, 4 ,5,6, 7. The dotted values of Fig. 6d represent the numerically computed root of the equation $R' = R'_{\lim}$ by varying parametrically $\bar{R}_1'$. In essence, these roots correspond to the value of the notch radius R' leading to R_1' estimations affected by a NCV value equal to ν. Interestingly, the points outline a trend converging to ν_0 for vanishing R' (infinintely sharp notch) that is well represented by the following expression (solid lines in Fig. 6d):

$$\nu = \nu_0\left(\bar{\alpha}\right) + n_1 \frac{R'}{\bar{R}_1'^{m_3(\bar{\alpha})}} + n_2 \frac{R'^2}{\bar{R}_1'^{m_4(\bar{\alpha})}} \tag{17}$$

Whose best-fit coefficients n_i are listed in Table 3. Equation (17) is very worthwhile, essentially for two reasons: (i) it permits to design the notch radius of the notch specimen according to the expected control radius R_1' and the desidered level of NCV ν; (ii) given the notch radius R' of the notched specimen used to estimate the the input value $\bar{R}_1'$ of the control radius, it is possible to calculate the NCV ν of R_1'. The knowledge of ν is useful to deduce the statistical properties of R_1'. In fact, the CV can be immediately estimated from Eq. (14); moreover, the expressions proposed in the following for evaluating mean and skewness at the above mentioned discrete values of ν (ν_0, 4, 5, 6, 7) can be extended to intermediate ν values through simple interpolation.

The results of MC simulations carried out to explore the effect of Σ and κ on mean and skewness are shown in Fig. 7a and b (dotted values), respectively. It is clear that increasing values of Σ and decreasing values of κ make more pronounced the asymmetry in the PDF of R_1'. This results in a progressive positive deviation of the mean μ from the input value $\bar{R}_1'$ and a concomitant increment in skewness *sk*. Hyperbolic functions (solid lines) are here proposed to interpolate the MC results plotted in Fig. 7. In particular, mean and skewness are well represented by the following expressions:

$$\frac{\mu}{\bar{R}_1'} = \cosh\left(\frac{\Sigma}{m_1\left(\bar{\alpha},\nu\right) + m_2\left(\bar{\alpha},\nu\right)\kappa}\right) \tag{18}$$

$$sk = \left(s_1\left(\bar{\alpha},\nu\right) + s_2\left(\bar{\alpha},\nu\right)\kappa\right)\sinh\left(\frac{\Sigma}{s_3\left(\bar{\alpha},\nu\right) + s_4\left(\bar{\alpha},\nu\right)\kappa}\right) \tag{19}$$

Whose best-fit coefficients m_i and s_i are listed in Table 5 and 6, respectively.

To conclude, Table 7 summarizes the validity range under which the proposed method to deduce the statistical properties of the inverse estimations of the control radius R_1' can be used with reasonable degree of approximation. The flowchart depicted in Fig. 8a summarizes the procedure for assessing the statistical properties of the control radius R_1'. This is also incorporated in Matlab scripts enclosed in the electronic version of the paper and described in the Appendix.

3.3 Probabilistic notch fatigue assessments

The statistical properties of the control radius deduced in the previous section can be used to estimate the uncertainty in the fatigue assessment of V-notches of severity different from that used for the inverse estimation of R_1. For this purpose, MC simulations were carried out to generate a skew-normally distributed population of R_1 with statistical parameters estimated according to the procedure illustrated in Fig. 8. Equations (7,8) are then used to calculate the corresponding notch fatigue factor K_f for a V-notched specimen of notch radius R'. Its fatigue strength is calculated within a probabilistic framework extracting individuals of K_f and

plain fatigue limit, this latter assumed as usual as normally distributed with mean $\Delta\bar{\sigma}_{\mathrm{fl}}$ and standard deviation *S*. The corresponding CV of the plain fatigue limit can be rearrenged from Eq. (13) as follows:

$$r = \frac{S}{\Delta\bar{\sigma}_{\mathrm{fl}}} = \frac{\Sigma}{\sqrt{\frac{1+\kappa^2}{2}}} \tag{20}$$

In this way, a population of notch fatigue strength is generated and its mean and standard deviation are finally evaluated. It was found that the mean is very well approximated by the following intuitive expression:

$$\Delta\bar{\sigma}_{\mathrm{N,fl}} = \frac{\Delta\bar{\sigma}_{\mathrm{fl}}}{K_{\mathrm{f}}\left(\mu\right)} \tag{21}$$

In other words, the mean notch fatigue strength is given by the ratio of the mean plain fatigue strength and the fatigue notch factor corresponding to the mean control radius μ (Eq. (18)).

Since the CV of the notch fatigue strength displays a nearly linear dependency upon the equivalent CV Σ of the input fatigue data, the following calculations will be expressed in terms of the NCV defined as $\frac{1}{\Sigma}\frac{S_{\mathrm{N}}}{\Delta\bar{\sigma}_{\mathrm{N,fl}}}$. The flowchart depicted in Fig. 8b summarizes the procedure for the probabilistic fatigue assessment of a notched geometry with diameter *D* notch radius *R* and opening angle $2\bar{\alpha}$ once the statistical properties of the control radius (namely mean μ, standard deviation δ and input value $\bar{R}_1'$) have been determined from an independent notch geometry (characterized by Σ and κ statistical properties).

The NCV estimated from MC simulations are shown in Fig. 9a-d (dotted values) for the four values κ comprised within the proposed validity range, namely 0.5, 1, 1.5 and 2, respectively, as a function of notch root radius R' and parametric in control radius R_1'. For the sake of brevity, Fig. 9 reports the simulations undertaken for ν =5. Similar trends are obtained for the remaining explored value of ν. Interestingly, these results indicate an asymptotic trend for large R_1' and small R_1' tending to the NCV of the plain fatigue strength (refer to Eq. 20) equal to $\frac{1}{\sqrt{\frac{1+\kappa^2}{2}}}$. For this reason, the following tri-variate fitting equation is proposed to represent the data shown in Fig. 9:

$$\frac{1}{\Sigma}\frac{S_{\mathrm{N}}}{\Delta\bar{\sigma}_{\mathrm{N,fl}}} = \sqrt{\frac{2}{1+\kappa^2}} + \frac{1}{\left(f_1\left(\bar{\alpha},\nu\right)+f_2\left(\bar{\alpha},\nu\right)\kappa\right)+\left(f_3\left(\bar{\alpha},\nu\right)+f_4\left(\bar{\alpha},\nu\right)\kappa\right)\frac{R'^2}{\bar{R}_1'^2}} \tag{22}$$

Whose best fit coefficients f_i are listed in Table 6. The agreement of this function (solid lines in Fig. 9) with the numerical data is very good. The aforementioned aysmptotic behavior is not surprising, as the notched specimen to be assessed tends to a smooth one for R' approaching infinity, especially for small values of the control radius R_1'. Looking at Fig. 9, it is also evident that NCV increases with increasing sharpness of the notch and is maximum for the perfectly sharp notch, regardless of the value of R_1'. As expected, NCV increases

with increasing ν. In particular, the maximum value achieved for the perfectly sharp notch increases from 1.8 at $\nu=\nu_0$ to 3.6 at $\nu=7$. Recalling the discussion started in the Introduction, this increment in NCV with respect to the smooth sample is related to the uncertainty in the control radius R_1', which in turn is linked to the inversion procedure (affecting mostly the sharpest notches) and to material's variability.

The statistical properties of R_1' and the probabilistic assessment of independent notch configurations discussed in this section will be applied in the following to interpret the fatigue data collected on two metallic materials.

4. Applicative examples

4.1 Experimental data

The experimental data derived from our previous papers [50,58] and [52,59] are analyzed with the proposed procedure. Specifically, in [50,58], the fatigue behavior of the Al aeronautical grade 7075-T6 (Poisson's ratio $\bar{\nu}=0.33$) was investigated by undertaking axial fatigue tests at two load ratios (R=-1 and R=0.1) on plain and notched specimens extracted from the same wrought bar. The geometry of this latter sample type is illustrated in Fig. 10a. In particular, notches of different acuity were machined. They differ in the notch root radius R: R0.12 (ultrasharp), R0.21 (sharp) and R1 (blunt). The first two types of notch proved to be suitable for reliable inverse search estimations of critical length L and control radius R_1, whereas the last was used for validation tests only. The interested reader is referred to [48,56] for further detail.

A specific point of novelty of the present work as compared to its companion paper [49] aimed at investigating the statistical properties of L is that the broader range of allowable values of Σ (see Table 7) permits to extend the statistical analysis to the outcomes of the investigations carried out in [52,59] on a new class of materials gaining growing interest in the academic and industrial field, viz. an additively manufactured (AM) Ti-alloy (Poisson's ratio $\bar{\nu}=0.30$). Such interest stems from the broad design freedom allowed by AM techniques and from the fact that they introduce defects into the material that are particularly critical to the fatigue structural integrity [60]. Specifically, notched samples, whose geometry is shown in Fig. 10b, were fabricated by selective laser melting (SLM) of the titanium alloy Ti-6Al-4V ELI (henceforth abbreviated Ti-64) and fatigue tested at the load ratio R=-1. To explore the defectiveness effect on the notch fatigue strength, two sample batches were fabricated. The first one, termed turned notch (T-N), is obtained by turning the notch from plain cylindrical bars, while in the second batch, termed SLM notch (SLM-N), the notch geometry is already introduced by the SLM process and a slight turning finish was applied to restore the correct notch radius. Notches of different severity were machined: samples with notch radius R0.2 (sharp) will be used for the inverse search of R_1, while those with notch radius R1 (blunt) will be used for verification.

The collected SN are shown in Fig. 11a and b for 7075-T6 and Ti-64, respectively, and are fitted according to the following asymptotic power law equation (solid lines):

$$\sigma_a = k_1 + \frac{k_2}{N_f^{k_3}} \tag{23}$$

Where σ_a is the amplitude (half range $\Delta\sigma$) stress and N_f the number of cycles to failure. The best-fit coefficients k_i are listed in Table 9 along with the estimated regression standard deviation S and S_N assumed to be uniform for the whole fatigue curve. In this way, it is possible to build the SN curves with 10% and 90% failure probability (dashed lines in Fig. 11).

As already discussed in [52], the fatigue stress concentration factor K_f used for the inverse search procedure of the AM Ti-64 is calculated by modifying the value of the plain fatigue strength to make it representative of the actual Vickers hardness and defect size leading to fatigue failure in the notched counterpart. In essence, as shown in Table 10, the population of critical defects was found to be different in the plain and notched specimens. This is due to the fact that the notch stress gradient forces the crack nucleation to occur in the vicinity of the notch apex; in this way, only a fraction of defects dispersed throughout the specimen volume have the potential to become critical, in contrast to the scenario present in smooth samples, wherein the uniform axial stress distribution in the gauge section is able to activate a larger fraction of defects. As a result, if the $\sqrt{area}$ Murakami model calibrated in [58] to account for the actual size of critical defects found in plain samples is applied to the population of critical defects found in the vicinity of the notch tip (listed in Table 10), the resulting fatigue strength is slightly different from that of the smooth samples. For this reason, the plain fatigue strength data reported in Table 9 and used in the following for the inverse estimation of R_1 slightly differ from those used to plot the SN curve of the original plain variant shown in Fig. 11b. The interested reader is referred to [52,61] for further detail.

4.2 Inverse search of the control radius R_1

Table 11 summarizes the results of the inverse search estimation of the control radius R_1 based on the high-cycle fatigue data listed in Table 9. It can be noted that all the experimental variants of 7075-T6 satisfy the requirements on Σ and κ listed in Table 7 for the validity of the proposed statistical analysis. The SLM Ti-64 variant displays a slight violation on the κ requirement, which was found to lead to consistent statistical results and will be therefore further developed in the present paper. Conversely, the turned Ti-64 variant is affected by significant deviations of both Σ and κ from the above-mentioned requirements, which make impossible the direct application of the devised statistical approach. An approximate way for overcoming this limitation will be discussed in the following.

Except for this last experimental condition, Table 11 lists the statistical properties of R_1 estimated according to Eq. (17-19). Table 11 reports also the results of MC simulations where, during each trial, R_1 is computed extracting normally distributed values of plain and notch fatigue strength with mean and standard deviation listed in Table 9. The agreement among the statistical parameters estimated in the two ways is satisfactorily good, especially for mean and CV δ/μ. As expected, the R_1 estimations made for 7075-T6 on the base of the ultrasharp (R0.12) notched geometry are affected by a lower value of NCV ν as compared to the predictions based on the sharp (R0.21) notch configuration. Regarding the Ti-64 SLM variant, the large value of R_1 in

comparison with the notch radius R makes the estimation of R_1 affected by a very low value of ν, viz. close to the minimum ν_0 attainable using a perfectly sharp notch.

Fig. 12a and b compare the PDF of R_1 estimated through MC simulations (histograms) and the SND with parameters deduced from Eqs. (17-19) and listed in Table 11 (solid curves) for 7075-T6 tested under R = −1 and R = 0.1, respectively, using the HCF data of the ultrasharp notched geometry. The agreement between the two approaches is very good. Fig. 12c illustrates the same PDF comparison for the Ti-64 SLM notch variant. Once again, the agreement is satisfactorily good, even though to a lower extent, probably due to the slight violation of the requirement on the maximum allowed κ value shown in Table 9.

Figure 13a illustrates the dependency of the control radius of Ti-64 upon the critical defect size. Besides the two AM variants here investigated, we consider a third experimental point (red dotted value) representative of the wrought counterpart under the same fine acicular microstructural conditions. Specifically, the control radius is deduced in this case from the fatigue limit and the crack growth threshold values found in the literature. The interested reader is referred to [52] for further detail. Interestingly, R_1 increases with the size of the critical defect and this trend is well represented by a hyperbolic tangent function (solid line in Fig. 13a). Figure 13b and c illustrates the SEM micrograph of critical defects typically found in the vicinity of the notch tip in the turned and SLM notched specimens, respectively. The aforementioned approximate method to estimate the statistical properties of R_1 of the turned notched variant is based on the assumption that the corresponding R_1 PDF can be obtained from that of the SLM variant by linearly scaling the only mean value and keeping the same CV and skewness. The comparison between this approximate estimation and that based on MC simulations incorporating the actual statistical properties of the input fatigue data is given in Fig. 12d. It can be noted that, despite the questionable assumption, the agreement between the two PDF is satisfactorily good. Therefore, the following probabilistic assessment of turned notches will be done considering this approximate statistical estimation of R_1.

The statistical analysis applied so far to the HCF strength can be then extended to the medium cycle fatigue regime. For this purpose, probabilistic notch assessments are made according to the flowchart depicted in Fig. 8b, wherein the plain fatigue strength and the control radius (which in turn is determined according to Fig. 8a from an independent notch variant) are random variables depending upon the number of cycles to failure. Once mean and standard deviation of the notch fatigue strength have been calculated, the SN curves can determined at different failure probability assuming the notch fatigue strength to be normally distributed.

Fig. 14a,c,e illustrate the dependency of mean (solid line), 10%,50%, 90% cumulative distribution function CDF (dashed lines) upon the number of cycles to failure N_f for 7075-T6 at R=0.1, for 7075-T6 at R=-1 and SLM Ti-64, respectively. It can be noted that R_1 decreases with increasing fatigue lives and that the almost symmetric PDF of 7075-T6 at R=-1 (see Fig. 12b) makes the distribution nearly Gaussian (mean and 50% CDF are practically coincident). Fig. 14b,d,f show the limit notch radius R_{lim} expressed by Eq. (16) as a function of N_f and parametric in the NCV ν. Interestingly, the ultrasharp notched configuration is able to keep ν between 4 and 5 and below 4 throughout the entire explored fatigue regime for 7075-T6 at R=0.1 and R=-1, respectively. Higher values of ν, though still within the validity interval, are obtained considering the sharp

notched geometry. For SLM Ti-64, ν is well below 4 throughout the entire fatigue regime thanks to the large R_1 to R ratio.

4.3 Probabilistic notch fatigue assessment

In this section, notch fatigue assessments are made through MC simulations and according to Eqs. (21-22) derived on the base of the statistical properties of the SND assumed for R_1.

Table 12 lists the results of the following self-consistency test: the statistical properties of R_1 inferred from a certain notched geometry are used to predict the fatigue strength (mean and standard deviation) of the same notch configuration. As expected, the mean value assessed according to both approaches is in very good agreement with the input value. More interestingly, both probabilistic assessments lead to a systematic overestimation of the standard deviation. The uncertainty linked to the inverse search procedure leads to an increased dispersion in the assessment of the input fatigue data.

Table 13 lists the results of the validation tests: fatigue assessments are made on notched configurations not used to get the statistical properties of R_1. The agreement in mean value is very good for all the investigated material variants, being the absolute relative error below 5%. Interestingly, when the ultrasharp notched geometry is used to assess independent notched configurations of 7075-T6, the standard deviation is very close to the experimental one for the blunt notch at both R ratios and sharp notch at R=-1, while it is overestimated for the sharp notch at R=0.1, wherein the uncertainty in R_1 is larger (ν is 4.6 vs 4 at R=-1). When the sharp notched geometry is used to get the statistical properties of R_1, the standard deviation of the blunt specimens is again in good agreement with the experimental data, whereas there is a systematic and significant overestimation of the standard deviation of the notched configurations that are sharper (ultrasharp) than that used for the R_1 inverse search procedure. This means that, in the former scenario, the uncertainty in fatigue predictions is mainly related to the material variability in plain fatigue strength and control radius R_1, whereas, in the latter one, it is primarily dictated by the uncertainty in the inverse search of R_1. The results of AMed Ti-64 further confirm these observations: the low NCV ν value in the estimation of R_1 makes the contribution of the uncertainty in inverse search of R_1 negligible and the standard deviation of the assessed variants is in very good agreement with the experimental values.

A careful reader may object that, in the case of R_1 estimations assessed by low NCV ν, the standard deviation of the fatigue notch assessments is mainly due to the dispersion in the plain fatigue strength data and consequently that no particular role is played by the material variability of R_1. However, if we look at Table 14, this is not exactly true. Indeed, Table 14 compares the CV of the plain fatigue strength with that of the notched variants, both deduced from experimental data and probability assessments. The experimental CV of the notched variants of 7075-T6 at R=0.1 is very close to that of the plain specimen tested under the same R. In this case, we can argue that the dispersion in the fatigue notch strength is actually due to the material variability in plain fatigue strength. The fact that the probabilistic notch fatigue assessment overestimates the actual CV, especially in the sharpest notch configuration, can be ascribed to the uncertainty introduced by the inverse search procedure. Different is the scenario depicted by 7075-T6 under R=-1. In this case, the low CV

value of the plain fatigue strength along with the lower uncertainty in R_1 (lower ν than at R=0.1) makes the probabilistic assessment of the CV of the notched (especially blunt) variants in better agreement with the experimental data as compared to the CV of the input plain fatigue strength. We expect therefore a non-negligible role of the material variability of R_1. Even more convincing is the situation displayed by the AMed Ti-64: the CV of the notched variants is significantly higher than that of the plain fatigue strength and is in much better agreement with that predicted by the probabilistic assessments. Apparently, the high level of defectiveness of this material class significantly increases the material variability of R_1 and this is correctly considered by the proposed statistical approach.

In conclusion, Fig. 15a-d compare the experimental data with the SN curves predicted on the base of the statistical distribution of R_1 shown in Fig. 14 as a function of N_f. The solid lines refer to 50% ($\Delta\bar{\sigma}_N$) failure probability, the dashed lines indicate 10% ($\Delta\bar{\sigma}_N - 1.282 \cdot S_N$) and 90% ($\Delta\bar{\sigma}_N + 1.282 \cdot S_N$) failure probability deduced from the knowledge of the standard deviation of the notch fatigue assessments. It can be noted that the proposed method allows for a sound rationalization of the experimental data: in fact, 80% of the experimental data lies within the 10%-90% dispersion band, apart from the predictions made for the sharp 7075-T6 notch at R=-1 (Fig. 15b): this mismatch is due to a slight underestimation of the mean fatigue strength (2%, see Table 13), whereas the amplitude of the dispersion band is coherent with that displayed by the experimental data.

5. Conclusions

The present paper investigated the statistical properties of the control radius R_1 estimated through the inverse search procedure proposed in [45]. This requires a specific notch geometry devised to minimize the sensitivity of R_1 to the experimental uncertainty. New fitting coefficients were proposed in this paper allowing for lower absolute relative errors with respect to [45]. Through Monte Carlo simulations, it was possible to demonstrate that, if the input quantities are normally distributed, the output variable has a non-symmetric probability density function that, under certain conditions, is well represented by a skew normal distribution. Approximate functions were proposed to predict mean, standard deviation and skewness of such distribution and tested using real experimental data. Probabilistic fatigue assessments were made on independent notch geometries. The following conclusions can be drawn:

1) The normalized coefficient of variation (NCV) of R_1 increases with increasing notch radius to R_1 ratio (Eq. 17). In this way, it is possible to design the acuity of the notched specimen to achieve the desired NCV of R_1.
2) The statistical properties of R_1 can be used for probabilistic fatigue assessments of notched geometries. The NCV in notch fatigue strength is dictated by two contributions, viz. the uncertainty in the plain fatigue strength and that in the control radius R_1. The former is predominant in materials with little dispersed control radius values and in blunt notch geometries.
3) The uncertainty in control radius can be thought as to be composed of two contributions: the uncertainty linked to the inverse search of R_1, particularly affecting the dispersion of the fatigue

assessment of very sharp notches, and the uncertainty linked to the material variability of notch sensitivity and hence in R_1. This last contribution plays a crucial role in additively manufactured materials, wherein the pronounced defectiveness amplifies the material variability of R_1.

4) Matlab scripts are attached to the on-line version of the present paper. They permit a fast inverse search of R_1 and the determination of its statistical properties. They can be used for probabilistic notch fatigue assessments, wherein Monte Carlo simulations are carried out by generating normally distributed plain fatigue strength and skew-normally distributed R_1 values.

Appendix

The compressed file `NewCoefficientsInverseDirect.zip` contains the text files listing in tabular form the coefficients c_{ij} and d_{ij} for inverse (Eq. (6)) and direct problems (Eq. (7)), respectively.

An example is reported in this appendix to show step-by-step the proposed statistical calculation procedure. The data analyzed here is about the experimental results of Aluminum alloy 7075-T6, under load ratio R = –1, and the Poisson's ratio for this alloy is $\bar{\nu} = 0.33$. This calculation sequence can be retrieved in the editable script files for MATLAB® software, which are available online in Appendix B. The script `RunThisFirst_SaveCoeffs.m` is initially required to be run, just to have all the coefficients available and saved in the local folder. The script `InverseSearchExample_StatisticalAnalysis.m` leads to the determination of the control radius, along with its statistical distribution and provides a graph for the PDF. The script `DirectProblemExample_StatisticalAnalysis.m` eventually allows the evaluation of the fatigue strength of another (blunter) specimen and the related standard deviation.

The SED control radius is initially determined by combining the *plain* specimen and the *ultrasharp* notched specimen, with their standard deviations. The fatigue strength properties are reported below, for the plain specimen:

$$\Delta\bar{\sigma}_{\mathrm{fl}} / 2 = 159\,\mathrm{MPa},\ S / 2 = 5.23\,\mathrm{MPa} \tag{A.1a}$$

and for the ultrasharp specimen, $D = 20\,\mathrm{mm}, \bar{\alpha} = 90°, R = 0.12\,\mathrm{mm}$:

$$\Delta\bar{\sigma}_{\mathrm{fl}} / 2 = 38.2\,\mathrm{MPa},\ S_{\mathrm{N}} / 2 = 2.19\,\mathrm{MPa} \tag{A.1b}$$

The plain and the notched specimen data can be combined, obviously to find the fatigue stress concentration factor:

$$K_{\mathrm{f}} = 4.162 \tag{A.2}$$

and by means of Eqs. (5) and (6) the control radius is obtained:

$$\bar{R}_1' = 0.005966 \tag{A.3a}$$

$$\bar{R}_1 = 0.05966\ \mathrm{mm} \tag{A.3b}$$

The coefficients of variation and the equivalent CV are easily found:

$$r = 0.03289 \tag{A.4a}$$

$$r_N = 0.05733 \tag{A.4b}$$

$$\kappa = 1.743 \tag{A.4c}$$

$$\Sigma = 0.04674 \tag{A.4d}$$

The normalized CV can be obtained from Eq. (17) resulting from the geometry of the notch (angle and dimensionless radius) and the obtained control radius in dimensionless form:

$$\nu = 3.989 \tag{A.5}$$

The mean value (dimensionless) μ of the control radius distribution can be obtained by interpolating Eq. (18):

$$\mu = \bar{R}_1' \cosh\left(\frac{\Sigma}{m_1(\bar{\alpha},\nu) + m_2(\bar{\alpha},\nu)\kappa} \right),\ \nu = \nu_0,...,7 \tag{A.6a}$$

and then by a piecewise linear interpolation it follows:

$$\mu(\nu = 3.989) = 0.005997 \tag{A.6b}$$

A similar procedure is followed to find the skewness of the distribution, according to Eq. (19):

$$sk = \left(s_1\left(\bar{\alpha},\nu\right) + s_2\left(\bar{\alpha},\nu\right)\kappa\right)\sinh\left(\frac{\Sigma}{s_3\left(\bar{\alpha},\nu\right) + s_4\left(\bar{\alpha},\nu\right)\kappa} \right),\ sk(\nu = 3.989) = 0.1590 \tag{A.7}$$

The standard deviation can be found by inverting Eq. (14):

$$\delta = \nu\,\mu\,\Sigma = 0.001118 \tag{A.8}$$

and the shape parameter α of the distribution is then obtained with Eq. (11e):

$$\alpha = \frac{1}{\sqrt{1 - sk^2}} \sum_{i=1}^{4} a_i\, sk^{i/2} = 1.103 \tag{A.9}$$

Now the scale parameter λ can be found by inverting Eq. (11c) since the values δ, α are available:

$$\gamma = \frac{\delta}{\sqrt{1 - \dfrac{2\alpha^2}{\pi(1+\alpha^2)}}} = 0.001386 \tag{A.10}$$

and the location parameter β is obtained with Eq. (11b):

$$\beta = \mu - \frac{\sqrt{\dfrac{2}{\pi}}\,\alpha\,\gamma}{\sqrt{1+\alpha^2}} = 0.005178 \tag{A.11}$$

All the parameters for the skew-normal PDF distribution are available now.

The strength of a blunter notched specimen (R = 1.0 mm) can be assessed with Eqs. (7), (8) and finally Eq. (21), and by using the mean value of the distribution for the control radius input. The fatigue stress concentration factor K_f is initially obtained, and then from the plain specimen fatigue stregth the assessment for the blunt notch is:

$$\mu \rightarrow \Delta\bar{\sigma}_{N,fl} / 2 = 63.5\,\text{MPa} \tag{A.12}$$

Eq. (22) eventually provides a calculation tool for the standard deviation, and an interpolation in terms of the CV is again required:

$$S_N = \Sigma\ \Delta\bar{\sigma}_{N,fl}\left(\sqrt{\frac{2}{1+\kappa^2}} + \frac{1}{\left(f_1(\bar{\alpha},\nu)+f_2(\bar{\alpha},\nu)\kappa\right)+\left(f_3(\bar{\alpha},\nu)+f_4(\bar{\alpha},\nu)\kappa\right)(R'/\bar{R}_1')^2}\right) \quad \text{(A.13a)}$$

By introducing the CV obtained with the mean value of the skewed distribution of the control radius, the resulting standard deviation is:

$$\nu = 3.982 \rightarrow S_N/2 = 2.23\,\text{MPa} \quad \text{(A.13b)}$$

Appendix B

Script files introduced in Appendix A for the online version of the paper:

```
RunThisFirst_SaveCoeffs.m
InverseSearchExample_StatisticalAnalysis.m
DirectProblemExample_StatisticalAnalysis.m
```

References

[1] Budynas RG, Nisbett JK. Shigley's mechanical engineering design. 10th ed. McGraw-Hill Education; 2014.

[2] Hanel B, Haiback E, Seeger T, Wirthgen G, Zenner H. Analytical strength assessment of components in mechanical engineering, Forschungskuratorium Maschinenbau (FKM). Frankfurt: VDMA Verlag; 2003.

[3] Götz S, Ellmer F, Eulitz KG. A fracture mechanics-based approach to estimating the endurance limit of notched components. Eng Fract Mech 2016;151:37–50.

[4] Vazquez J, Navarro C, Dominguez J. A model to predict fretting fatigue life including residual stresses. Theoret Appl Fract Mech 2014;73:144–51.

[5] Neuber H. Theory of notch stresses: principles for exact calculation of strength with reference to structural form and material. second ed. Berlin: Springer;1958.

[6] Peterson RE. Notch sensitivity. In: Sines G, Waisman JL, editors. Metal fatigue. New York: McGraw Hill; 1969. p. 293–306.

[7] Liao D, Zhu SP, Correia J, De Jesus A, Berto F. Recent advances on notch effects in metal fatigue. Fatigue Fract Eng Mater Struct 2020;43:637–659.

[8] Taylor, D. (2007) The theory of critical distances: a new perspective in fracture mechanics. Elsevier Science. ISBN: 9780080444789.

[9] Susmel L. A unifying approach to estimate the high-cycle fatigue strength of notched components subjected to both uniaxial and multiaxial cyclic loadings. Fatigue Fract Eng Mater Struct 2004;27(5):391–411.

[10] Yao WX. Stress field intensity approach for predicting fatigue life. Int. J. Fatigue. 1993;15(3):246-246.

[11] Shang DG, Wang DK, Li M, Yao WX. Local stress-strain field intensity approach to fatigue life prediction under random cyclic loading. Int. J. Fatigue. 2001;23(10):903-910.

[12] Zhang CC, Yao WX. Typical fatigue life analysis approaches for notched components. J Aerosp Power 2013;28(6):1223–30.

[13] Sih GC. Strain-energy-density factor applied to mixed mode crack problems. Int J Fract 1974;10:305–21.

[14] Gillemot LF. Criterion of crack initiation and spreading. Eng Fract Mech 1976;8:239–53.

[15] Lazzarin P, Zambardi R. A finite-volume-energy based approach to predict the static and fatigue behavior of components with sharp V-shaped notches. Int J Fract 2001;112(3):275–98.

[16] Livieri P, Lazzarin P. Fatigue strength of steel and aluminium welded joints based on generalised stress intensity factors and local strain energy values. Int J Fract 2005;133(3):247–76.

[17] Lazzarin P, Berto F. Some expressions for the strain energy in a finite volume surrounding the root of blunt V-notches. Int J Fract 2005;135(1–4):161–85

[18] Lazzarin P, Sonsino C, Zambardi R. A notch stress intensity approach to assess the multiaxial fatigue strength of welded tube-to-flange joints subjected to combined loadings. Fatigue Fract Eng Mater Struct 2004;27(2):127–40.

[19] Susmel L. Modified Wöhler curve method, theory of critical distances and Eurocode 3: a novel engineering procedure to predict the lifetime of steel welded joints subjected to both uniaxial and multiaxial fatigue loading. Int J Fatigue 2008;30:888–907.

[20] Vantadori S, Fortese G, Ronchei C, Scorza D. A stress gradient approach for fretting fatigue assessment of metallic structural components. Int J Fatigue;2017;101:1-8.

[21] Muthu J. Fatigue life of 7075-T6 aluminium alloy under fretting condition. Theoret Appl Fract Mech 2014;74(1):200-208.

[22] Gates N, Fatemi A. Multiaxial variable amplitude fatigue life analysis using the critical plane approach, Part II: Notched specimen experiments and life estimations. Int J Fatigue 2018;106:56-69.

[23] Liao D, Zhu SP, Q G. Multiaxial fatigue analysis of notched components using combined critical plane and critical distance approach. Int J Mechanical Sciences 2019;160:38-50.

[24] Hu Z, Berto F, Susmel L. The strain energy density to estimate lifetime of notched components subjected to variable amplitude fatigue loading. Frattura ed Integrità Strutturale 2019;47(1): 383-393.

[25] Benedetti M, Fontanari V, Allahkarami M, Hanan J, Bandini M. On the combination of the critical distance theory with a multiaxial fatigue criterion for predicting the fatigue strength of notched and plain shot-peened parts. Int J Fatigue 2016;93:133–47.

[26] Benedetti M, Berto F, Marini M, Raghavendra S, Fontanari V. Incorporating residual stresses into a Strain-Energy-Density based fatigue criterion and its application to the assessment of the medium-to-very-high-cycle fatigue strength of shot-peened parts. Int J Fatigue 2020;139:105728.

[27] Benedetti M, Santus C. Mean stress and plasticity effect prediction on notch fatigue and crack growth threshold, combining the theory of critical distances and multi- axial fatigue criteria. Fatigue Fract Eng Mater Struct 2019;42(6):1228–46.

[28] Liao D, Zhu SP. Energy field intensity approach for notch fatigue analysis. Int J Fatigue 2019;127:190–202.

[29] ISO EN 1993, Eurocode 3: design of steel structures. 2005.

[30] FKM Guideline, Analytical strength assessment of components in mechanical engineering. 2012.

[31] Muñiz-Calvente M, Blasón S, Fernández-Canteli A, de Jesus A, Correia J. A probabilistic approach for multiaxial fatigue criteria. Frattura ed Integrità Strutturale 2016;11(39):160–165.

[32] Gallegos Mayorga L, Sire S, Correia J, De Jesus A, Rebelo C, Fernández-Canteli A, Ragueneau M, Plue B. Statistical evaluation of fatigue strength of double shear riveted connections and crack growth rates of materials from old bridges. Eng Fract Mech 2017;185:241-257.

[33] Correia J, Apetre N, Arcari A, De Jesus A, Muñiz-Calvente M, Calçada R, Berto F, Fernández-Canteli A. Generalized probabilistic model allowing for various fatigue damage variables. Int. J. Fatigue 2017;100:187–194.

[34] Barbosa JF, Correia J, Freire Junior RCS, De Jesus A, Fatigue life prediction of metallic materials considering mean stress effects by means of an artificial neural network. Int. J. Fatigue 2020;135:105527.

[35] Ai Y, Zhu S-P, Liao D, Correia JAFO, De Jesus AMP, Keshtegar B. Probabilistic modelling of notch fatigue and size effect of components using highly stressed volume approach. Int J Fatigue 2019;127:110–9.

[36] Zhu SP, Foletti S, Beretta S. Probabilistic framework for multiaxial LCF assessment under material variability. Int J Fatigue 2017;103:371-385.

[37] Fatemi A, Socie DF. A critical plane approach to multiaxial fatigue damage including out-of-phase loading. Fatigue Fract Eng Mater Struct 1988;11(3):149–65.

[38] Liu X, Wang R, Hu D, Mao J. A calibrated weakest-link model for probabilistic assessment of LCF life considering notch size effects. Int J Fatigue 2020;137: 105631.

[39] Klawonn A, Hagenacker A, Beck T. A probabilistic Haigh diagram based on a weakest link approach. Int J Fatigue 2020;133:105419

[40] Pessard E, Bellett D, Morel F, Koutiri I. A mechanistic approach to the Kitagawa-Takahashi diagram using a multiaxial probabilistic framework. Eng. Fract. Mech. 2013;109:89–104.

[41] Owolabi GM, Prasannavenkatesan R, McDowell DL. Probabilistic framework for a microstructure-sensitive fatigue notch factor. Int J Fatigue 2010;32:1378–1388.

[42] Jha SK, John R, Larsen JM. Incorporating small fatigue crack growth in probabilistic life prediction: Effect of stress ratio in Ti–6Al–2Sn–4Zr–6Mo. Int J Fatigue 2013;51:377–388.

[43] Karlén K, Olsson M, Ahmadi H, Härkegård G. On the effect of random defects on the fatigue notch factor at different stress ratios. Int J Fatigue 2012;41:179–187.

[44] Santus C, Taylor D, Benedetti M. Determination of the fatigue critical distance according to the Line and the Point Methods with rounded V-notched specimen. Int J Fatigue 2018;106:208–218.

[45] Benedetti M, Santus C, Berto F. Inverse determination of the fatigue Strain Energy Density control radius for conventionally and additively manufactured rounded V- notches. Int J Fatigue 2019;126:306–18.

[46] ASTM, Standard Test Method for Measurement of Fatigue Crack Growth Rates, ASTM E647 – 15; 2015.

[47] Forth S, Newman J, Forman R. On generating fatigue crack growth thresholds. Int J Fatigue 2003;25(1):9–15.

[48] Petit J, Zeghloul A. On the effect of environment on short crack growth behaviour and threshold. In: Miller K, de los Rios E, editors, The behaviour of short fatigue cracks, EGF Pub. 1, Mechanical Engineering Publications: London; 1986. p. 163–77.

[49] Benedetti M, Santus C. Statistical properties of threshold and notch derived estimations of the critical distance according to the line method of the theory of critical distances. Int J Fatigue 2020;137:105656.

[50] Santus C, Taylor D, Benedetti M. Experimental determination and sensitivity analysis of the fatigue critical distance obtained with rounded V-notched specimens. Int J Fatigue 2018;113:113–25.

[51] Taylor D, Hughes M, Allen D. Notch fatigue behaviour in cast irons explained using a fracture mechanics approach. Int J Fatigue 1996;18(7):439–45.

[52] Benedetti M, Santus C. Notch fatigue and crack growth resistance of Ti-6Al-4V ELI additively manufactured via selective laser melting: a critical distance approach to defect sensitivity. Int J Fatigue 2019;121:281–92.

[53] Strutz T. Data Fitting and Uncertainty (A practical introduction to weighted least squares and beyond). 2nd edition, Springer Vieweg, Berlin, 2016, ISBN 978-3-658-11455-8.

[54] Rice RC. Fatigue data analysis. In: Kuhn H, Medlin D, editors. ASM Handbook 2000 Vol. 8 Mechanical Testing and Evaluation. ASM International. doi: 10.31399/asm. hb.v08.9781627081764.

[55] Nadarajah S. Distribution properties and estimation of the ratio of independent Weibull random variables. AStA Adv Stat Anal 2010;94:231–246 https://doi.org/10.1007/s10182-010-0134-1.

[56] Azzalini A, Capitanio A. The skew-normal and related families. Cambridge University Press; 2013.

[57] Díaz-Francés E, Rubio FJ. On the existence of a normal approximation to the distribution of the ratio of two independent normal random variables. Stat Pap 2012;54(2):309–23. https://doi.org/10.1007/s00362-012-0429-2.

[58] Benedetti M, Berto F, Le Bone L, Santus C. A novel Strain-Energy-Density based fatigue criterion accounting for mean stress and plasticity effects on the medium-to-high-cycle uniaxial fatigue strength of plain and notched components. Int J Fatigue 2020;133:105397.

[59] Benedetti M, Fontanari V, Bandini M, Zanini F, Carmignato S. Low- and high-cycle fatigue resistance of Ti-6Al-4V ELI additively manufactured via selective laser melting: mean stress and defect sensitivity. Int J Fatigue 2018;107:96–109.

[60] Masuo H, Tanaka Y, Morokoshi S, Yagura H, Uchida T, Yamamoto Y, et al. Influence of defects, surface roughness and HIP on the fatigue strength of Ti-6Al-4V manufactured by additive manufacturing. Int J Fatigue 2018;117:163–79.

[61] Benedetti M, Santus C. Building the Kitagawa-Takahashi diagram of flawed materials and components using an optimized V-notched cylindrical specimen. Eng. Fract. Mech. 2020;224:106810.

Tables

Table 1. Coefficients for the singularity-based analysis of the V-notched specimen.

$2\bar{\alpha}$	s	$K_{N,UU}$	I_1			m		
			$\bar{\nu}=0.27$	$\bar{\nu}=0.30$	$\bar{\nu}=0.33$	$\bar{\nu}=0.27$	$\bar{\nu}=0.30$	$\bar{\nu}=0.33$
90°	0.455516	0.3210	0.81715	0.77192	0.72467	0.97352	0.98043	0.98884
60°	0.487779	0.2866	0.84387	0.79271	0.73898	0.96829	0.97696	0.98745

Table 2. a_i fit model coefficients for the inversion of Eq. (11e).

a_1	a_2	a_3	a_4
2.6159	1.7983	-5.4302	4.1124

Table 3: Best-fit coefficients of the equations used to estimate NCV of R_1' (Eq. (17)).

Notch angle $2\bar{\alpha}$	NCV	Best-fit coefficients of Eq. (17)			
	ν_0	n_1	n_2	n_3	n_4
90°	3.140	0.2752	0.1434	0.8776	1.991
60°	2.932	0.02478	0.3012	1.398	1.832

Table 4: Best fit coefficients of the equations used to estimate R_1' (Eq. (15))

Notch angle $2\bar{\alpha}$	NCV	b_1	b_2
90°	4	0.4721	-0.3740
	5	0.3129	-0.09226
	6	0.2480	-0.06302
	7	0.2052	-0.05047
60°	4	0.4248	-0.3045
	5	0.2964	-0.1084
	6	0.2410	-0.1047
	7	0.1993	-0.09003

Table 5: Best fit coefficients of the equations used to estimate mean value of R_1' (Eq. (18)).

Notch angle $2\bar{\alpha}$	NCV	Symbol	Index i	
			1	2
90°	ν_0	m_i	0.2411	0.07261
	4		0.2238	0.1369
	5		0.1868	0.1980
	6		0.1534	0.2458
	7		0.1253	0.2869

60°	ν_0		0.2501	0.08307
	4		0.2139	0.2091
	5		0.1678	0.2784
	6		0.1349	0.3209
	7		0.1050	0.3514

Table 6: Best fit coefficients of the equations used to estimate skewness of R_1' (Eq. (19))

Notch angle $2\bar{\alpha}$	NCV	Symbol	Index *i*			
			1	2	3	4
90°	ν_0	s_i	0.5591	0.1828	0.03268	0.05253
	4		0.6043	-0.1182	0.04643	0.04272
	5		0.5267	-0.1877	0.04761	0.03725
	6		0.5237	-0.2469	0.05305	0.03300
	7		0.4374	-0.2388	0.04692	0.03297
60°	ν_0		0.8930	0.05799	0.05580	0.05351
	4		0.6043	-0.1182	0.04643	0.04272
	5		0.4729	-0.2170	0.04880	0.03624
	6		0.4823	-0.2562	0.05195	0.03796
	7		0.4340	-0.2548	0.05155	0.03379

Table 7. Requirements for statistically validated R_1' estimations.

Requirements on input fatigue data	Requirement on R_1'	Requirements on R'
$\Sigma \le 0.1$ $0.5 \le \kappa \le 2$	$0.0025 \le R_1' \le 0.08$	$R' \le 0.2$

Table 8: Best fit coefficients for the estimation of the normalized standard deviation on the estimation of notch fatigue limit (Eq. (22)).

Notch angle $2\bar{\alpha}$	NCV	Symbol	Index *i*			
			1	2	3	4
90°	ν_0	f_i	1.632	-0.2932	0.1962	-0.04946
	4		1.094	-0.1704	0.1251	-0.03004
	5		0.7728	-0.1032	0.08236	-0.01867
	6		0.5906	-0.06887	0.05964	-0.01278
	7		0.4822	-0.05800	0.04632	-0.01074

60°	ν_0		1.600	-0.2875	0.2112	-0.05244
	4		0.9615	-0.1424	0.1181	-0.02750
	5		0.6828	-0.08592	0.07906	-0.01751
	6		0.5328	-0.06643	0.05867	-0.01377
	7		0.4300	-0.04811	0.04475	-0.01004

Table 9. Fatigue data used for inverse statistical estimation of the control radius R_1.

Material	R	Geometry	k_1 (MPa)	k_2 (MPa)	k_3	Fatigue life	$\Delta\bar{\sigma}_{fl}/2$ $\Delta\bar{\sigma}_{N,fl}/2$ (MPa)	$S/2$ $S_N/2$ (MPa)	CV
Al 7075-T6	0.1	plain	114.8	62347	0.651	3×10^7	116	9.4	0.08
		notch *R*0.12	24.67	81852	0.742		24.9	1.46	0.06
		notch *R*0.21	26.48	32560	0.638		27.0	1.43	0.06
	-1	plain	158.3	946747	0.810		159	5.23	0.03
		notch *R*0.12	38.01	2.6010×10^7	1.101		38.2	2.19	0.06
		notch *R*0.21	36.15	3078	0.364		42.0	2.69	0.06
Ti-64 SLM	-1	plain	240*	123927	0.646	5×10^7	241.5*	14*	0.06
		notch *R*0.2	109.7	60374	0.514		116.3	15.2	0.13
Ti-64 Turned		plain	185*	123927	0.646		186.5*	12.4*	**0.07**
		notch *R*0.2	72.0	496.0	0.144		110.5	18.0	**0.16**
* Estimated according to the Murakami model devised in [43,50] to account for the actual critical defect size in the notched specimens.									

Table 10. Hardness and critical defect size in plain and sharp notched variants of additively manufactured Ti-6Al-4V investigated in [52,59].

Material/geometry	Hardness $HV_{0.1}$	Critical defect size $\sqrt{area}_{max}$ (μm)	
		Mean	Standard deviation
Plain	382	150	61.4
SLM sharp notch	401	63	22.6
Turned sharp notch	385	223	78.6

Table 11. Statistical properties of the inverse estimation of the control radius R_1. Data in bold indicate violation of the requirements set in Table 7.

Material	R	Geom.	$\bar{R}_1$ (mm)	Σ	κ	ν	Monte Carlo			Predictions Eq. (17-19)		
							$\mu/\bar{R}_1$	δ/μ	*sk*	$\mu/\bar{R}_1$	δ/μ	*sk*
Al 7075-T6	0.1	*R*0.12	0.04338	0.071	0.72	4.57	1.024	0.317	0.503	1.023	0.324	0.461
		*R*0.21	0.03892	0.068	0.65	7.86	1.012	0.534	0.217	1.023	0.538	0.272
	-1	*R*0.12	0.05966	0.047	1.74	3.99	1.006	0.179	0.205	1.005	0.186	0.159
		*R*0.21	0.06587	0.051	1.95	5.01	1.004	0.255	0.070	1.004	0.247	0.050
Ti-64 SLM	-1	*R*0.2	0.1178	0.101	2.26	3.85	1.026	0.374	0.413	1.02	0.389	0.312
Ti-64 Turned		*R*0.2	0.1934	**0.124**	**2.45**	3.49	1.047	0.407	0.735	*	*	*
* not compliant with the requirements set by Table 7.												

Table 12. Self-consistency tests: probabilistic HCF assessment of notch geometries used to get R_1.

Material	R	Geometry	Exp. (MPa)		Monte Carlo (MPa)		Eq. (21-22) (MPa)	
			$\Delta\bar{\sigma}_{N,fl}/2$	$S_N/2$	$\Delta\bar{\sigma}_{N,fl}/2$	$S_N/2$	$\Delta\bar{\sigma}_{N,fl}/2$	$S_N/2$
Al 7075-T6	0.1	*R*0.12	24.9	1.46	25.2	3.30	25.4	3.35
		*R*0.21	27.0	1.43	27.2	3.61	27.3	3.68
	-1	*R*0.12	38.2	2.19	38.5	2.76	38.5	2.92
		*R*0.21	42.0	2.69	42.3	3.31	42.3	3.48
Ti-64 SLM	-1	*R*0.2	116.3	15.2	116.7	18.0	117.0	19.4

Table 13. Validation tests: probabilistic HCF assessment of independent notch geometries.

Material	R	Start. geometry	Pred. geometry	Exp. (MPa)		Monte Carlo (MPa)		Eq. (21-22) (MPa)	
				$\Delta\bar{\sigma}_{N,fl}/2$	$S_N/2$	$\Delta\bar{\sigma}_{N,fl}/2$	$S_N/2$	$\Delta\bar{\sigma}_{N,fl}/2$	$S_N/2$
Al 7075-T6	0.1	*R*0.12	*R*1	45.0	2.72	45.5	3.77	45.5	3.77
			*R*0.21	27.0	1.43	27.9	2.98	27.9	3.02
		*R*0.21	*R*1	45.0	2.72	45.3	3.84	45.3	3.82
			*R*0.12	24.9	1.46	24.1	4.58	24.5	4.47
	-1	*R*0.12	*R*1	62.3	2.86	63.5	2.21	63.5	2.23
			*R*0.21	42.0	2.69	41.2	2.39	41.2	2.49
		*R*0.21	*R*1	62.3	2.86	64.0	2.42	64.0	2.40
			*R*0.12	38.2	2.19	39.8	3.91	39.9	4.13
Ti-64 SLM	-1	*R*0.2 SLM	*R*1	148.8	17.2	145.5	14.4	144.8	15.0
Ti-64 Turned			*R*0.2	110.5	18.0	112.2	20.9	110.5	19.9
			*R*1	116.6	11.8	124.5	17.1	122.4	12.0

Table 14. Coefficient of variation of experimental data and predictions of independent notch geometries. Comparison with the experimental CV of the plain specimen variant. Data in bold indicates bad estimation of actual CV of notched variants

Material	R	Start. geometry	Pred. geometry	CV			
				Plain	Exp.	Monte Carlo	Assessment from Eq. (21-22)
Al 7075-T6	0.1	*R*0.12	*R*1	0.08	0.06	0.08	0.08
			*R*0.21		0.05	**0.11**	**0.11**
		*R*0.21	*R*1		0.06	0.08	0.08
			*R*0.12		0.06	**0.19**	**0.18**
	-1	*R*0.12	*R*1	**0.03**	0.05	**0.03**	0.04
			*R*0.21		0.06	0.06	0.06
		*R*0.21	*R*1		0.05	0.04	0.04
			*R*0.12		0.06	**0.10**	**0.10**

Ti-64 SLM	-1	*R*0.2 SLM	*R*1	**0.06**	0.12	0.10	0.10
Ti-64 Turned			*R*0.2	**0.06**	0.16	0.19	0.18
			*R*1		0.10	0.14	0.10

Figures

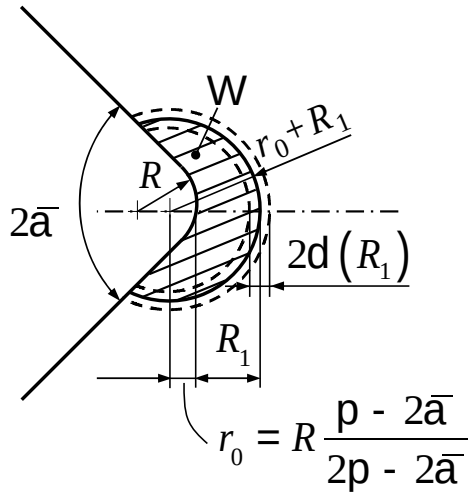

Figure 1. Strain energy density averaging domain Ω ahead of the notch root. $\delta(R_1)$ indicates the amplitude of the uncertainty interval of the control radius R_1, which is the focus of the present paper.

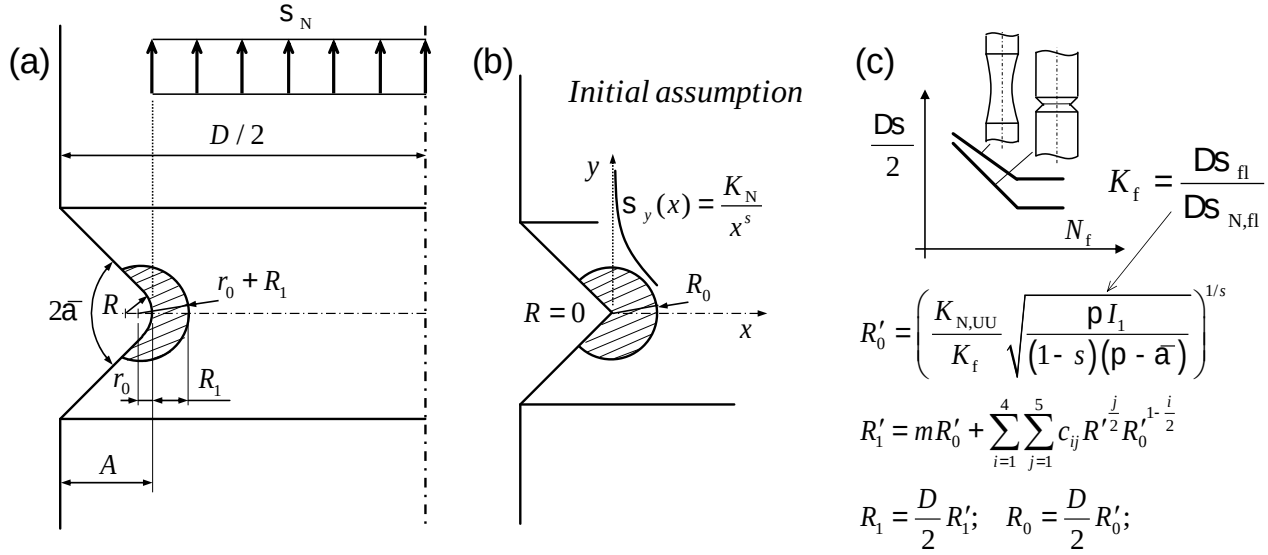

Figure 2. (a) Specimen geometry for notch-derived estimation of the control radius R_1. (b) Initial assumption based on singular stress distribution. (c) summary of the control radius inverse search.

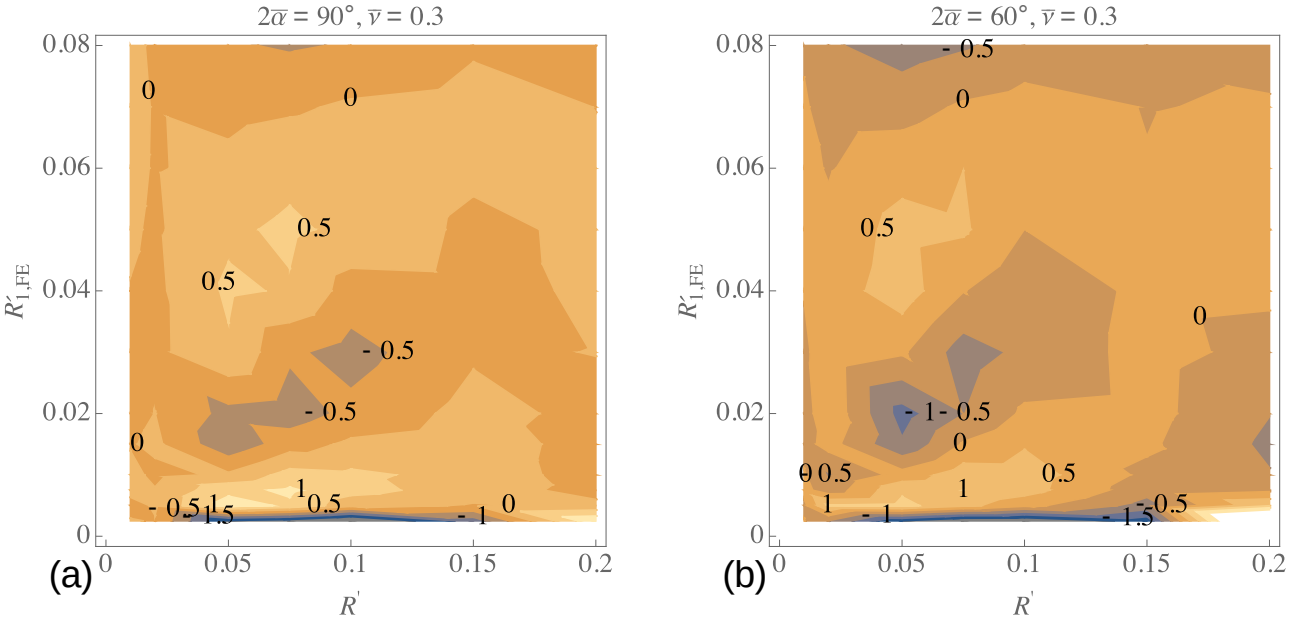

Figure 3. Percentage relative difference between the FE control radius and the inverse search procedure result for the opening angle $2\bar{\alpha} = 90°$ (a) and $2\bar{\alpha} = 60°$ (b). The new fitting technique proposed in the present paper allows for a reduction in maximum absolute relative error with respect to [45].

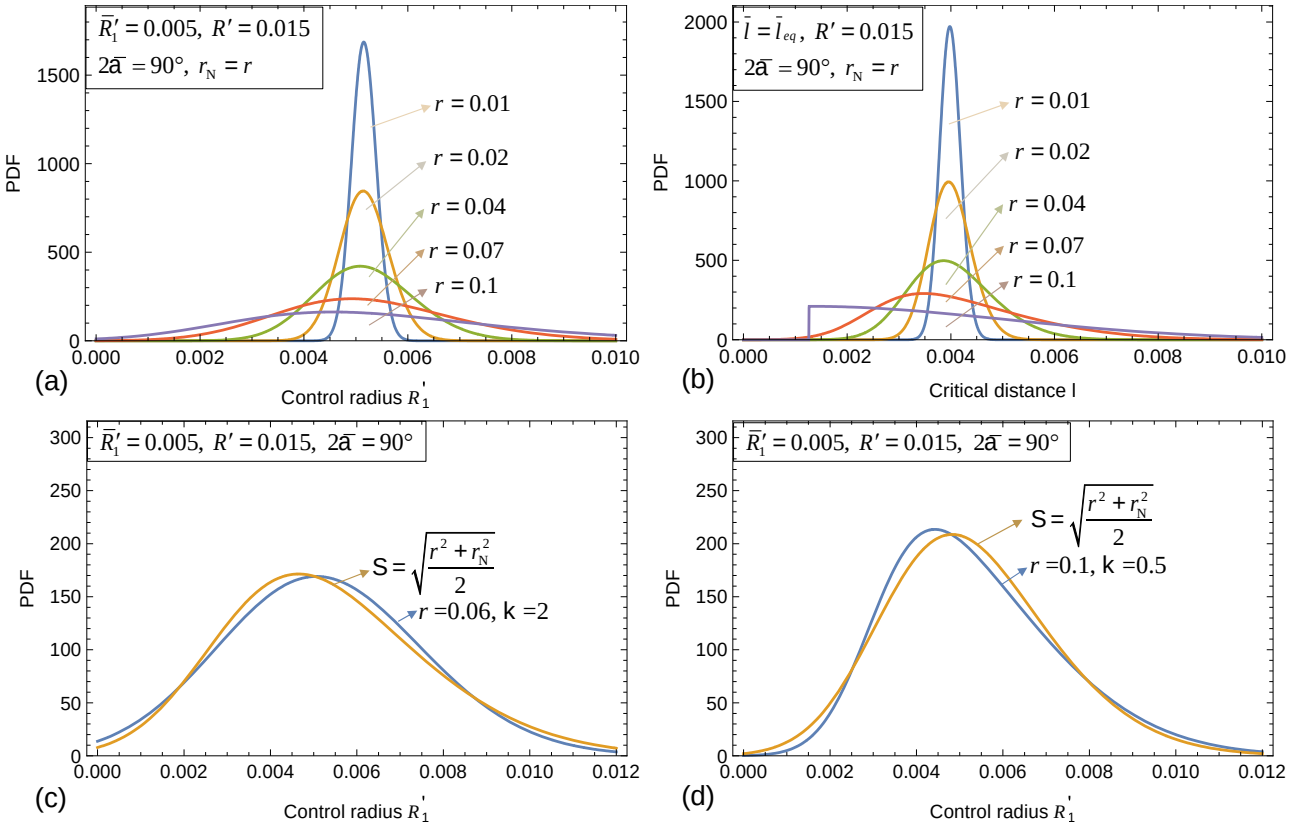

Figure 4. (a) Probability density function (PDF) of notch-derived control radius estimations. Histograms are obtained from Monte Carlo (MC) simulations. Mean, standard deviation and skewness calculated from MC simulations are used to evaluate the parameters of the skew-normal distributions plotted as solid lines. *r* is the coefficient of variation (CV) of the plain fatigue strength, which is here assumed to be equal to CV of the

notch fatigue strength (r_N). (b) PDF of notch-derived critical distance corresponding the same notch fatigue factor as that considered in (a). (c) and (d) PDFs accounting for the effective CV, r, $r_N = \kappa\, r$, are compared with those obtained considering, for plain and notch fatigue strength, the same equivalent CV, namely Σ. (c) maximum, (d) minimum value of the validity range established for κ.

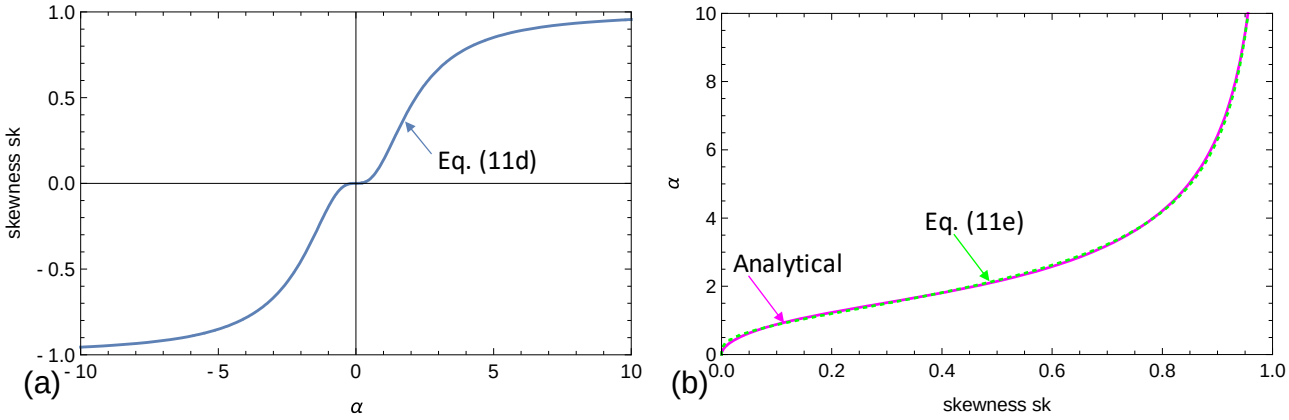

Figure 5. (a) relation between skewness and shape parameter α for the skew-normal distribution (Eq. (11d)). (b) comparison between analytical and numerical (Eq. (11e), dotted yellow line) inversion of Eq. (11d).

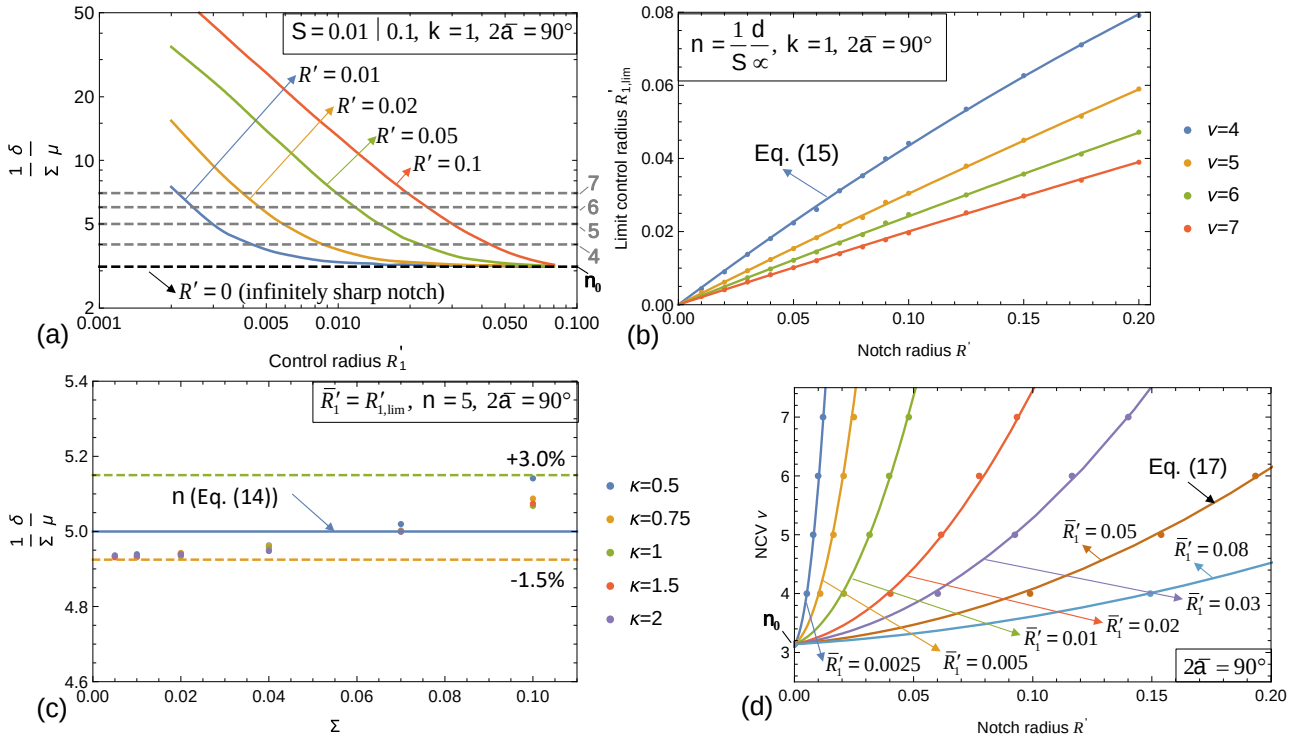

Figure 6. (a) The CV of notch-derived R_1' estimations normalized to Σ (and denoted as ν) depends on the notch radius R'. Here, the statistical properties of R_1' will be evaluated considering five values of ν, ranging from ν_0 (corresponding to an infinitely sharp notch, black dashed line) to 7. (b) $R_{1,\mathrm{lim}}'$ is the *locus* of control radii for varying notch radii R' corresponding to a certain value of ν. (c) The NCV ν for the *locus* $R_{1,\mathrm{lim}}'$ is

fairly independent of Σ and R' within an error band −1.5%, 3%. (d) The dependency of ν upon R' and R_1' is well represented by Eq. (17).

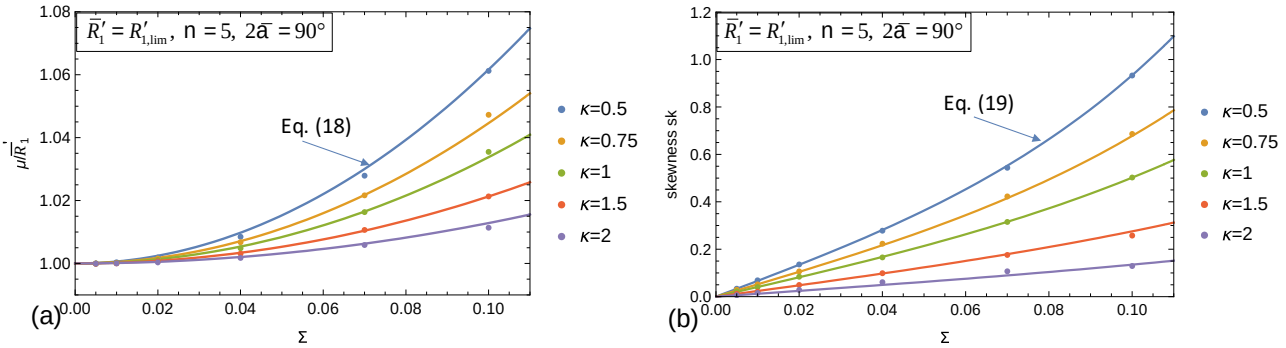

Figure 7. Statistical properties of notch-derived R_1' estimations characterized by the same ν value (here taken equal to 5). (a) Mean to input $\bar{R}_1'$ ratio and (b) skewness are well represented by hyperbolic functions Eq. (18-19).

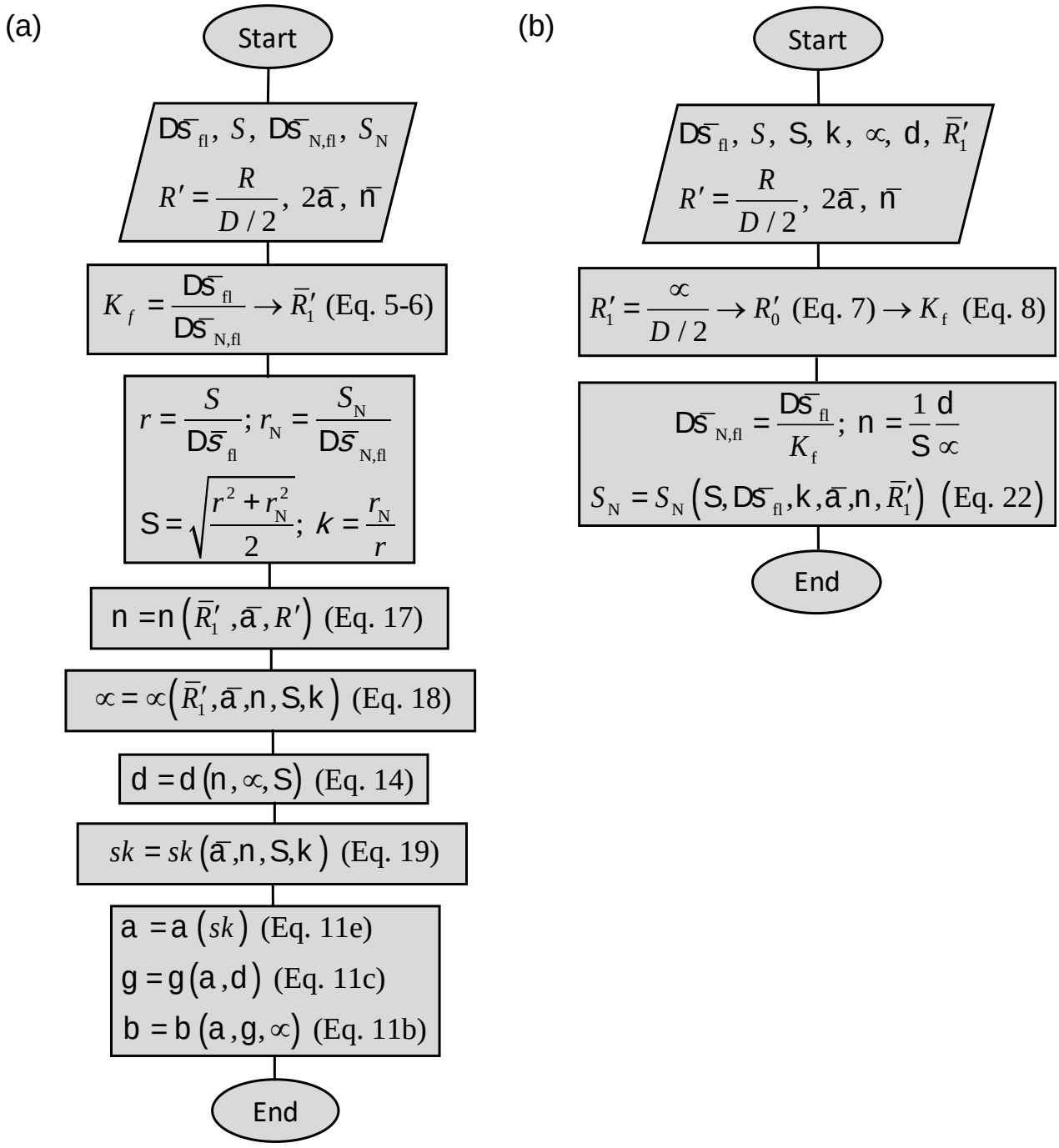

Figure 8. (a) Flowchart illustrating the step-by-step calculation procedure of the statistical properties of notch-derived control radius estimations. (a) Flowchart illustrating the probabilistic fatigue notch assessment taking into account the statistical properties of the control radius R_1.

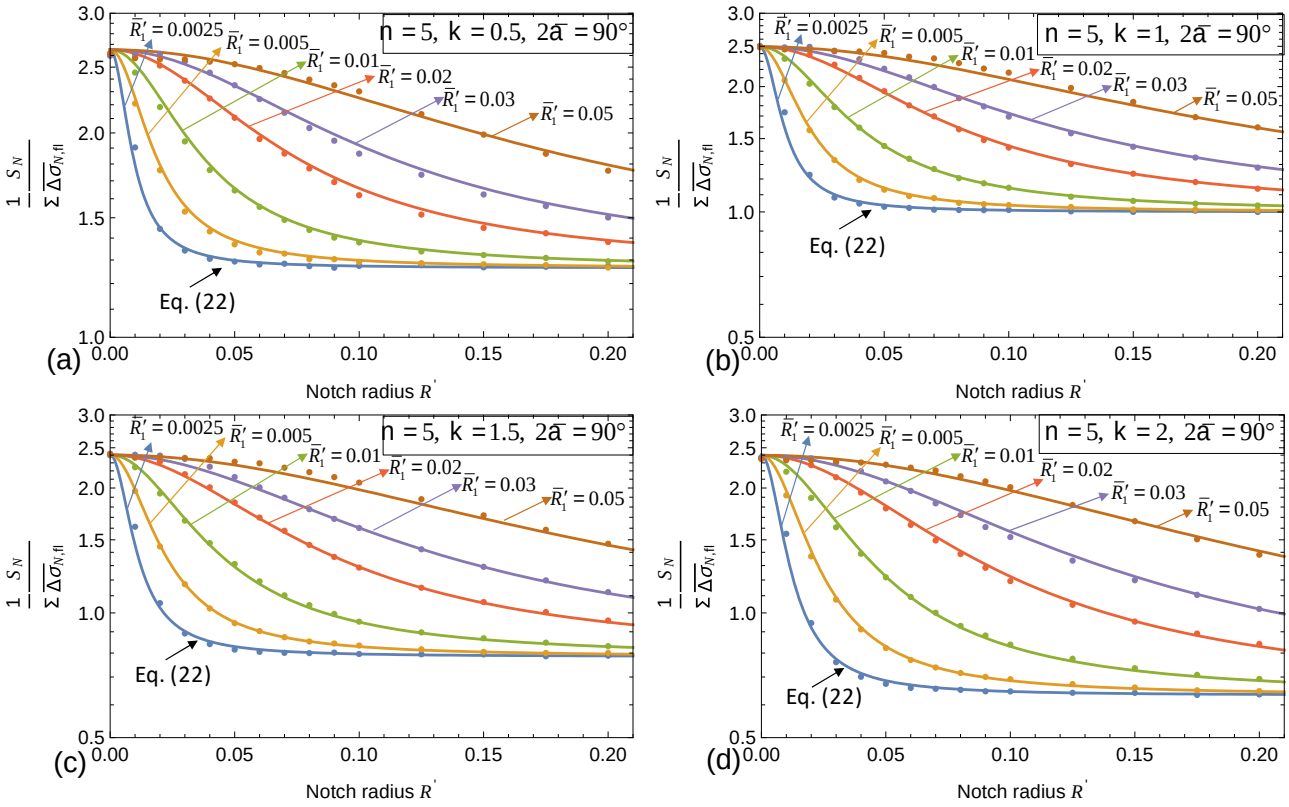

Figure 9. Dependency of the CV of notch fatigue strength estimations made using notch-derived control radius estimations upon notch radius R' and input control radius $\bar{R}_1'$. The plots are build considering the value of NCV ν=5. Similar trends were obtained for all the explored values of ν. (a) κ=0.5, (b) κ=1, (c) κ=1.5, (d) κ=2. The results of MC simulations (dotted values) are well represented by Eq. (22) (solid lines).

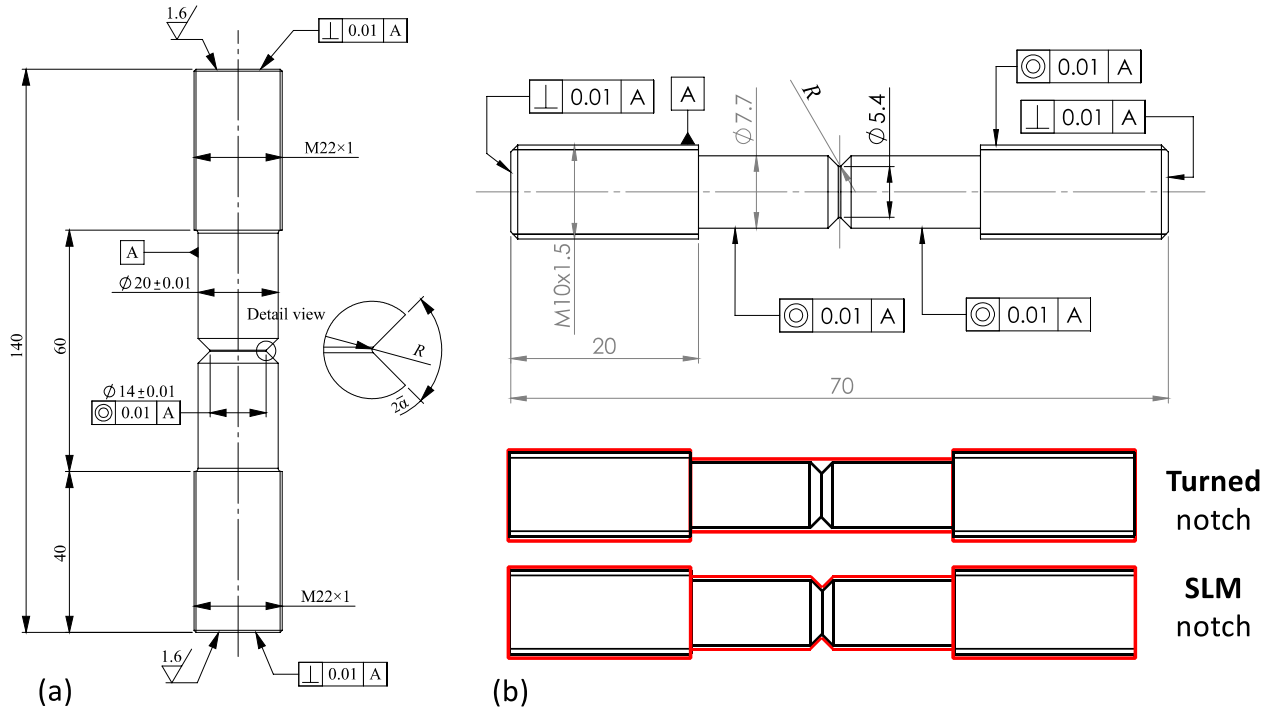

Figure 10. Geometry of notched specimens used in the present study. (a) Specimens of Al 7075-T6 were fatigue tested in [50,58]. Three different notch radii R were explored: R0.12 (ultrasharp), R0.21 (sharp), R1 (blunt). (b) Specimens of Ti-6Al-4V were additively manufactured and fatigue tested in [52]. Two different notch radii R were explored: R0.2 (sharp), R1 (blunt). Notches were fabricated directly via selective laser melting (SLM notch) or by turning additively manufactured cylindrical bars (Turned notch).

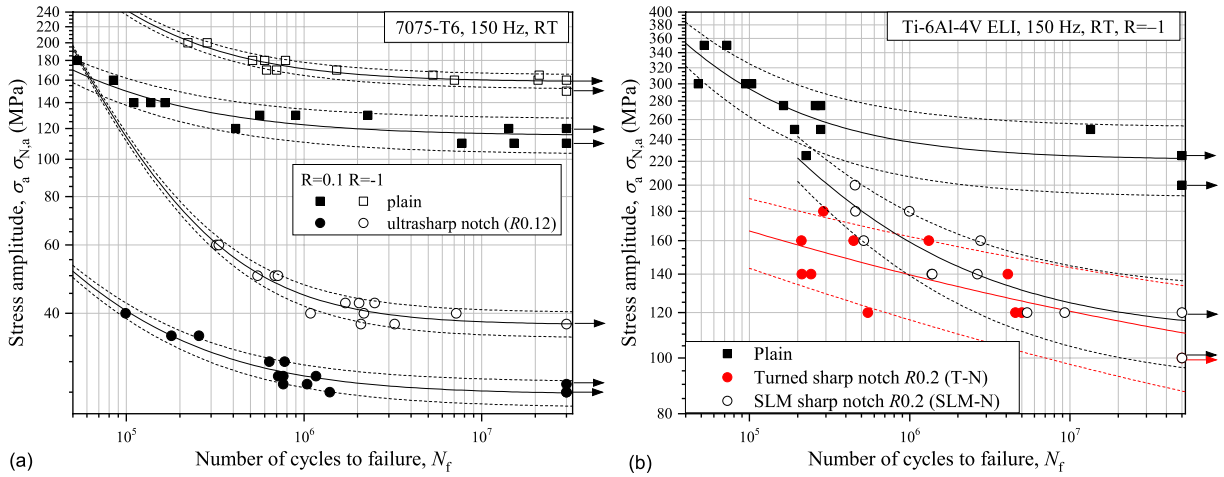

Figure 11. SN curves of plain and notched specimens used for the inverse search estimation of R_1. (a) Al 7075-T6, (b) additively manufactured Ti-6Al-4V. Solid lines refer to 50% failure probability, dashed lines to 10% and 90% failure probability. Arrows indicate run-out tests.

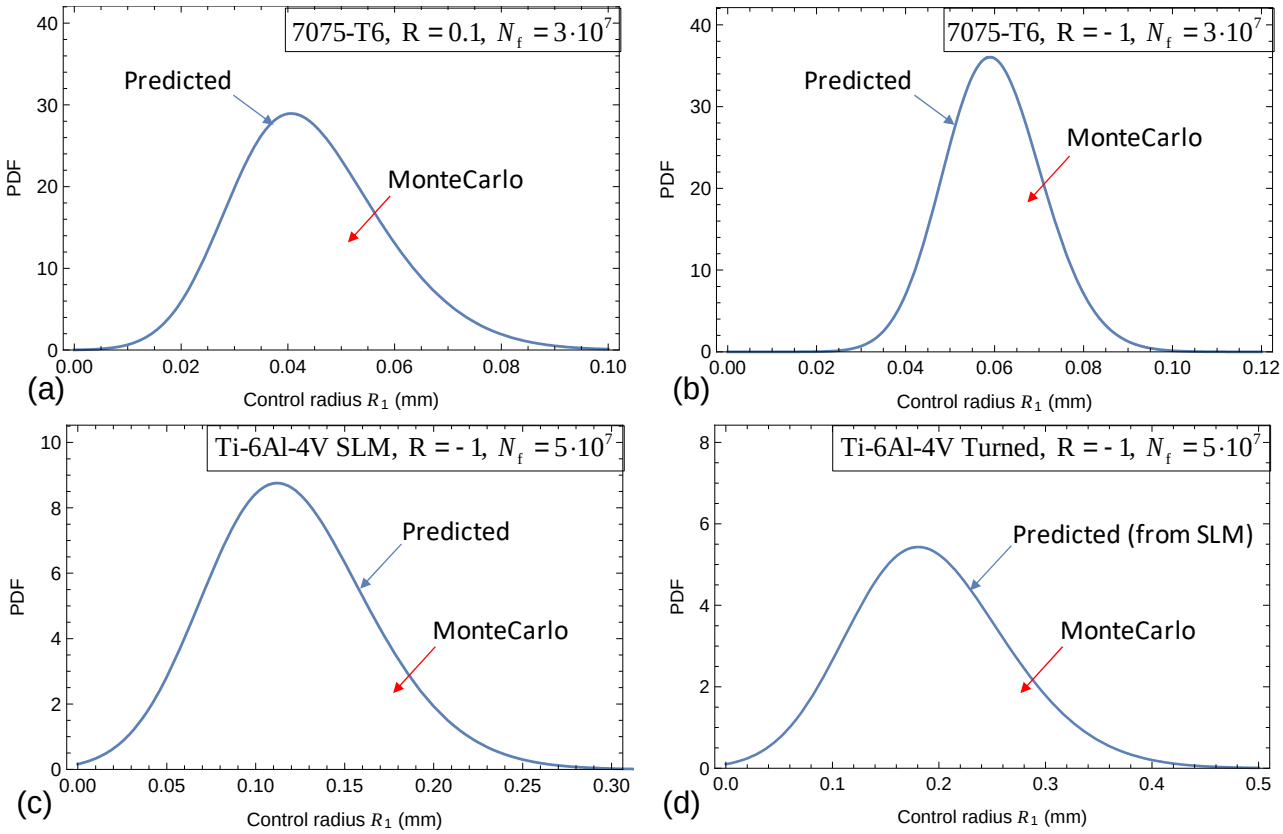

Figure 12. Comparison between PDF estimated through MC simulations and predicted by Eqs. (17-19) for the notch-derived control radius. (a) Al 7075-T6 tested at R=0.1, (b) Al 7075-T6 tested at R=-1, (c) Ti-6Al-4V where the notch was directly fabricated via SLM, (d) Ti-6Al-4V where the notch was turned from SLMed bars. In (d) the PDF is predicted from that shown in (c) by scaling the mean value according to Fig. 13.

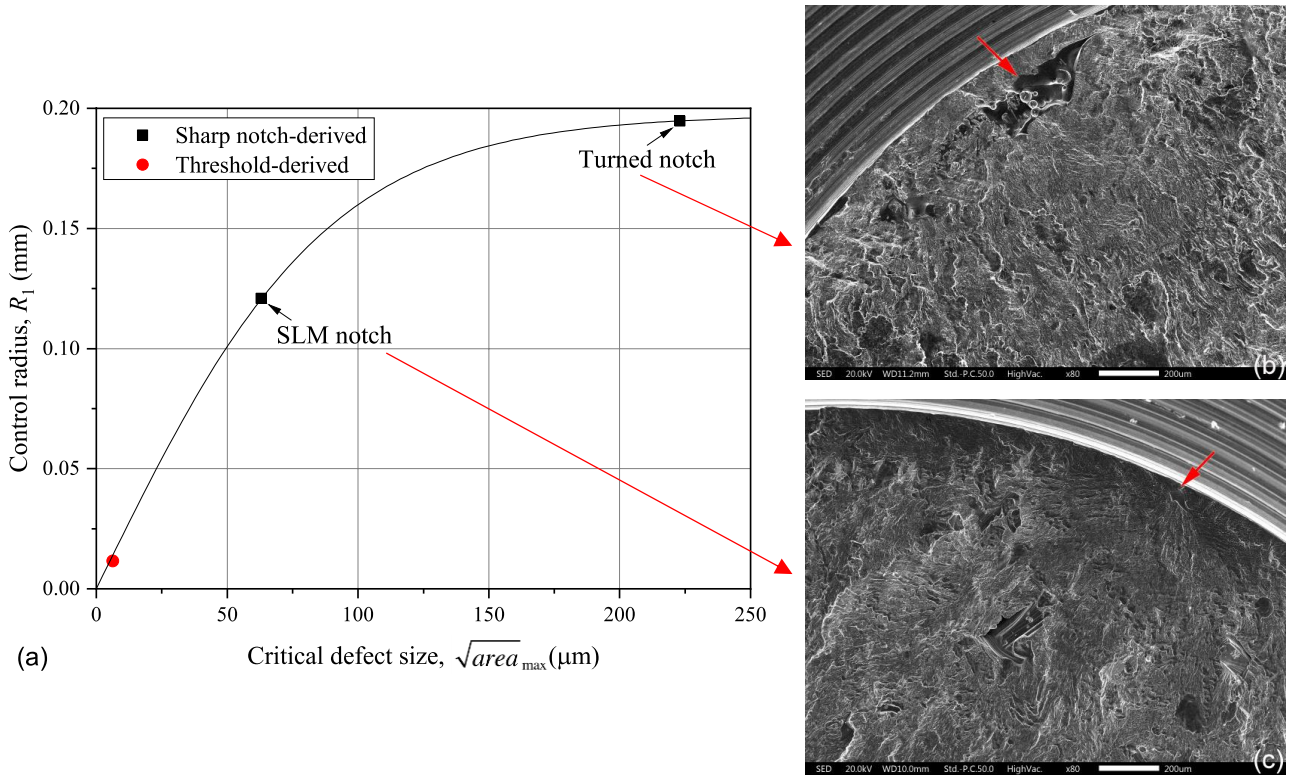

Figure 13. (a) Control radius dependency upon the critical defect size from experimental data collected in [50] for additively manufactured Ti-6Al-4V and from the literature for a conventionally processed material with similar microstructure. (b) and (c) SEM micrograph of the fracture surface illustrating (red arrows) the critical defect in the vicinity of the tip of turned and SLM notch, respectively. The solid line indicates the hyperbolic tangent function proposed in [52].

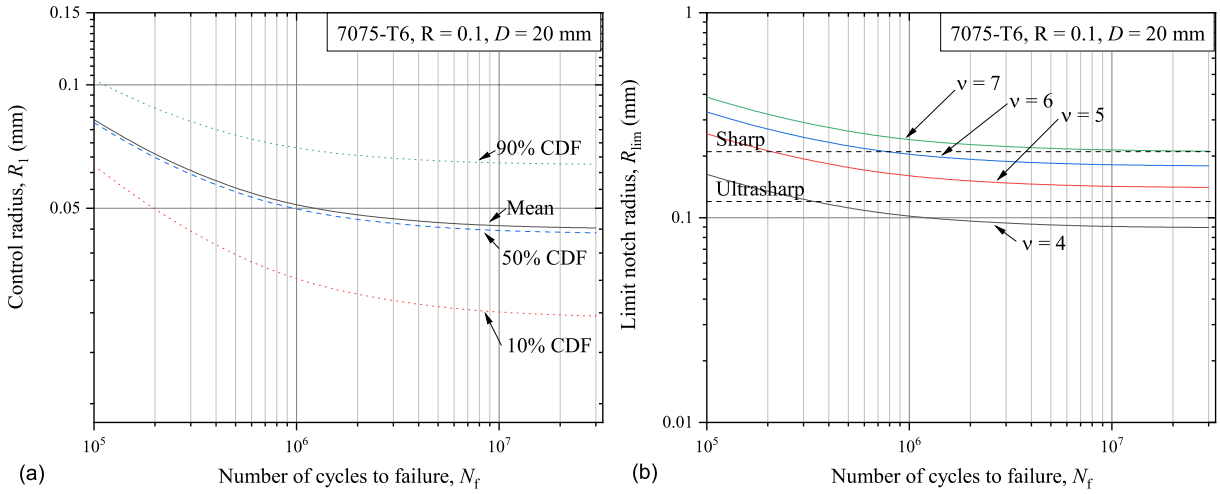

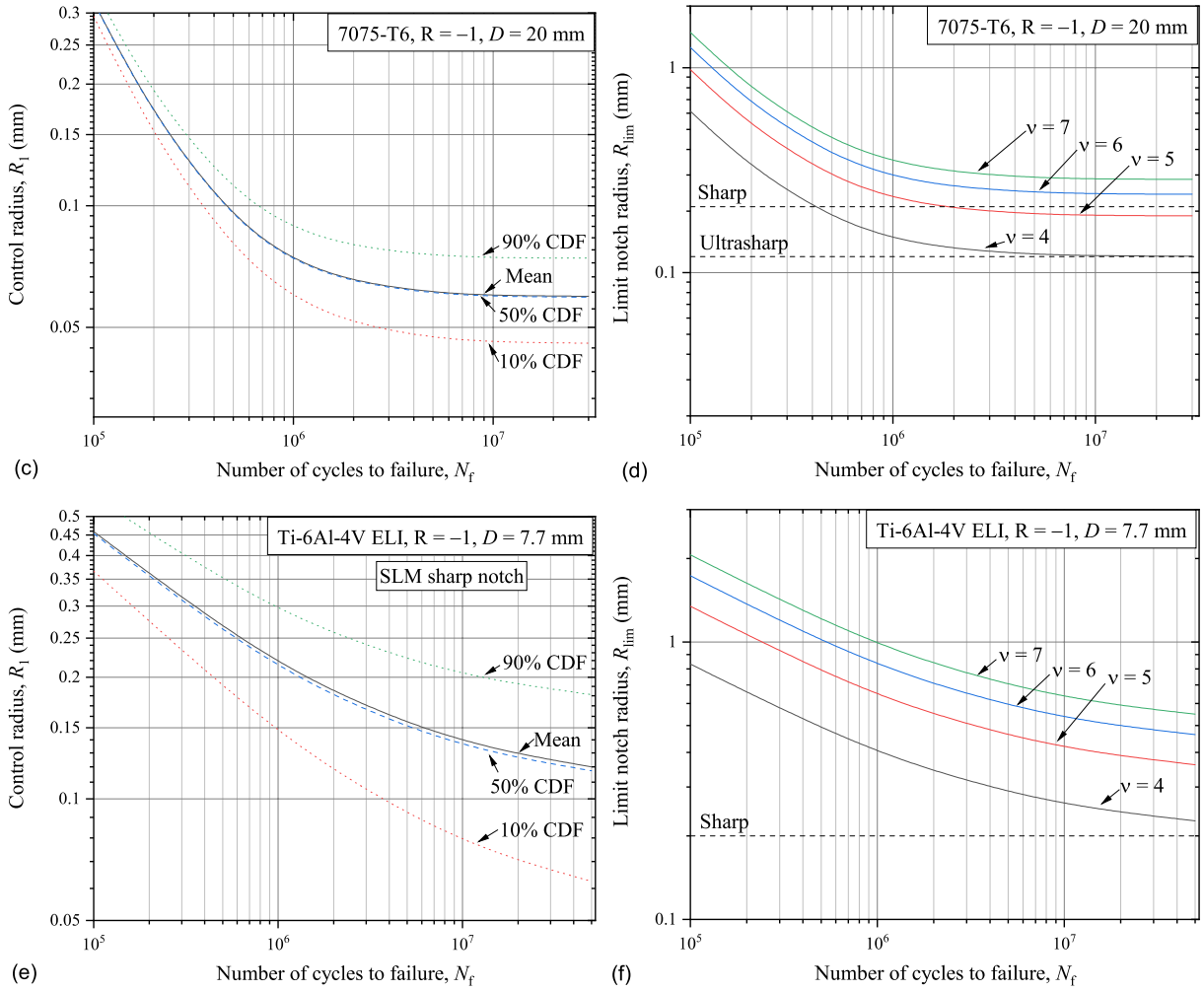

Figure 14. (a), (c), (e) Results of the inverse search statistical determination of the control radius as a function of the number of cycles to failure for (a) Al 7075-T6 at R=0.1, (c) Al 7075-T6 at R=-1, (e) Ti-6Al-4V where the notch was directly fabricated via SLM. (b), (d), (f) Limit notch radius R_{lim} (Eq. (16)) as a function of the number of cycles to failure. (a)-(b) Al 7075-T6 at R=0.1, (c)-(d) Al 7075-T6 at R=-1, (e)-(f) Ti-6Al-4V where the notch was directly fabricated via SLM.

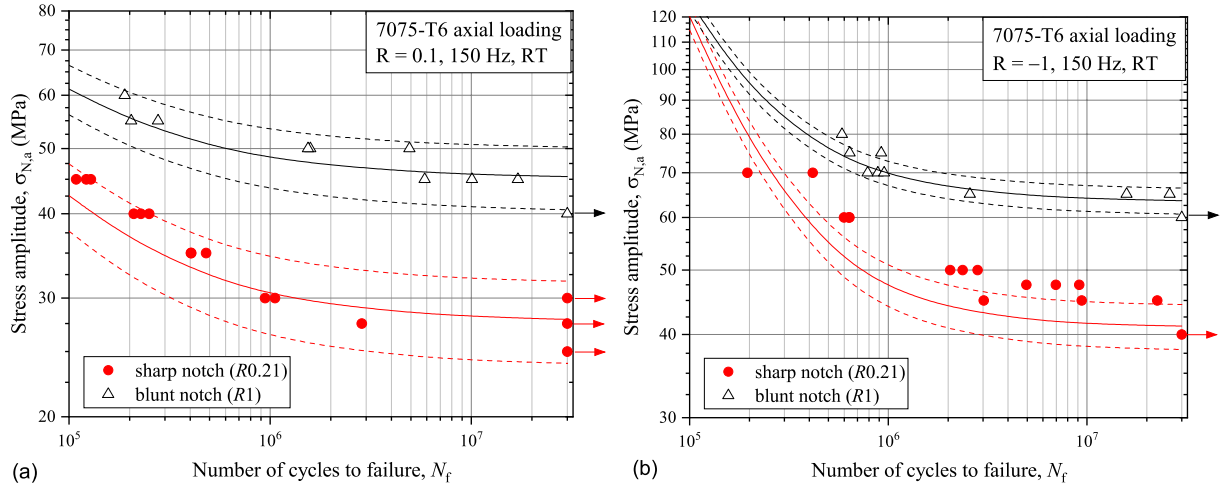

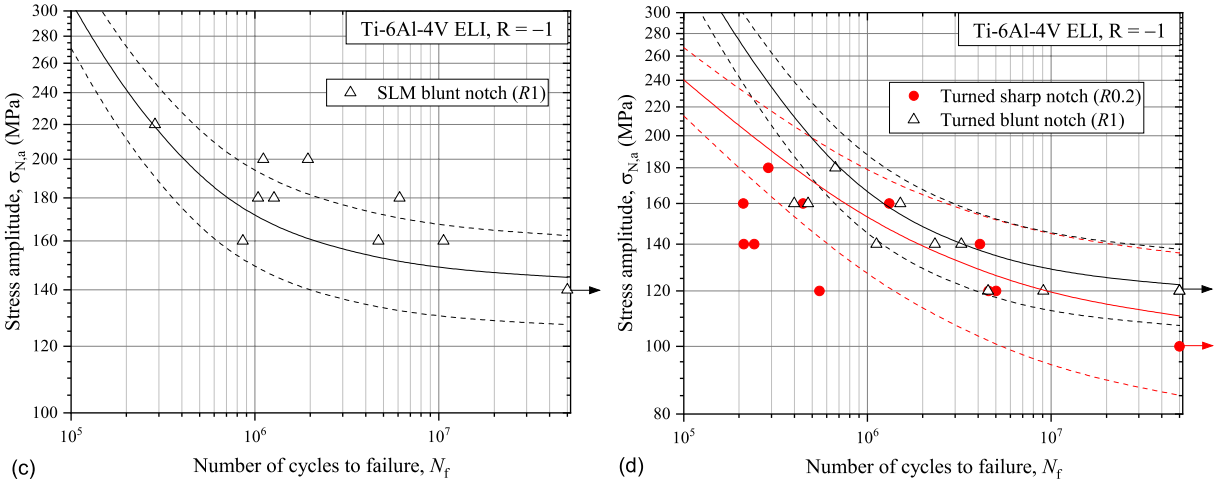

Figure 15. Probabilistic assessment of SN curves of independent notch geometry not used for R_1 inverse estimation. Solid lines refer to 50% failure probability, dashed lines to 10% and 90% failure probability. Dotted values are experimental results. (a) Al 7075-T6 at R=0.1, (b) Al 7075-T6 at R=-1, (c) Ti-6Al-4V where the notch was directly fabricated via SLM, (d) Ti-6Al-4V where the notch was machined by turning AMed cylindrical bars.